A Multi-scale Simulation Scheme to Investigate Dynamics of Membrane Confined Polymer

A thesis submitted towards partial fulfilment of
BS-MS Dual Degree Programme

by

Shibananda Das

under the guidance of

Dr. Apratim Chatterji
Assistant Professor, IISER Pune

Indian Institute of Science Education and Research
Pune

Certificate

This is to certify that this thesis entitled "A Multi-scale Simulation Scheme to Investigate Dynamics of Membrane Confined Polymer" submitted towards the partial fulfilment of the BS-MS dual degree programme at the Indian Institute of Science Education and Research Pune represents original research carried out by "Shibananda Das" at "IISER Pune", under the supervision of "Dr. Apratim Chatterji" during the academic year 2013-2014.

Student
Shibananda Das

Supervisor
Dr. Apratim
Chatterji

Acknowledgements

I would like to thank my thesis supervisor, Dr. Apratim Chatterji, for his guidance and support. It was a great learning experience working under his guidance. I am also grateful for his role in triggering my interest in the area of soft-matter physics.

Thanks are due to Mubeena and Mainak with whom fruitful dicussions led only to improvements to this project.

Thanks to my friends here at IISER Pune, with whom I have spent the most memorable five years of my life.

I would like to thank my parents for their support and always encouraging me.

I also forward my thanks to IISER Pune and DST, Govt. of India for providing facilities and support during these five years.

Abstract

This thesis describes a coarse grained multi-scale simulation technique to study the dynamics of a polymer suspended in fluid bounded by two fluctuating surfaces. In our study, these two surfaces are represented as membrane with stochastic height undulations. First, the simulation model of individual components, the membrane, the fluid and the polymer were implemented and validated by observing their characteristic physical properties. Then they were coupled to each other taking into account the interaction between each individual component. The fluctuation spectrum $S(q)$ of a membrane in the absence and in the presence of a confined fluid was obtained; $S(q)$ follows a q^{-4} dependence in the small q regime for both cases. The mean square displacement and end-to-end vector correlation were calculated for the polymer coupled to the fluid. The diffusion of polymer with $D \propto t$ was observed for long time scales.

This thesis primarily focuses on the development and implementation of the simulation scheme. The next step (work in progress) is obviously to do a detailed study of the three component system in the immediate future.

Contents

Chapter 1

Introduction

Membranes and polymeric molecules are the basic constituents of biological soft-matter systems. Thermal fluctuations play an important role in affecting their conformations because of the energy cost for their shape fluctuations are a few times k_BT. In the last few decades, there has been many detailed studies of the physics of membranes and polymers using methods of statistical mechanics; theoretical models describing the statics and dynamics of individual systems are well established. The physics of membranes is also of interest to the larger physics community as the physics of fluctuating surfaces floating in a fluid [1]. Modelling the dynamics of such fluctuating surfaces poses the challenge of calculating moving boundary conditions surrounding a fluid volume.

The polymer-membrane interaction has been of great interest and the effects of polymer adhesion to membrane is well studied in literature [2, 3, 4, 5]. The conformational changes arising from polymer-membrane interaction are relevant to biological functions such as cell fusion, cytoskeletal modulation and biopolymer folding in membranes.

The properties of self-avoiding polymers under confinement are also well understood. Daoud and de Gennes described the relaxation dynamics of a self-avoiding polymer with constrained geometries using simple scaling arguments [6, 7]. This scaling theory has been extended to the study of polymers under various confinements [8, 9, 10, 11, 12, 13] because of its relevance to several biological phenomena such as DNA translocation, bacterial chromosome segregation, and proteins confined between cell membranes. Furthermore, confined polymers are encountered in numerous applications like DNA sequencing, viral injection and drug delivery techniques.

1.1 Thesis outline and motivation

The research work presented in this thesis involves the study of a system comprised of a polymer suspended in a liquid under confinement by two membranes. In general one can also consider the membranes to be fluctuating surfaces with bending rigidity κ. The membrane surfaces undergo shape undulations due to thermal fluctuations and there is a constant hydrodynamic interaction between the membranes and the polymer mediated by fluid. In our study, we desire to find out how the membrane shape-fluctuations affect the dynamics and structure of the suspended polymer. The main focus of this work was to set up a simulation scheme to study the system consisting of polymer, membrane and fluid interacting with each other.

The membrane was modeled as a dynamically triangulated surface, multi-particle collision dynamics (MPCD) simulation secheme was used as a coarse grained model for the fluid and the polymer was modeled as bead-spring chain. Physical properties of the three components were validated separately with theory and then they were coupled with each other taking hydrodynamic interaction into consideration. Next, we describe in brief the preliminary results of our study of the suspended polymer as it interacts with the membrane surface due to momentum transport through the fluid, as well as due to the local flow of fluid trapped between fluctuating surfaces.

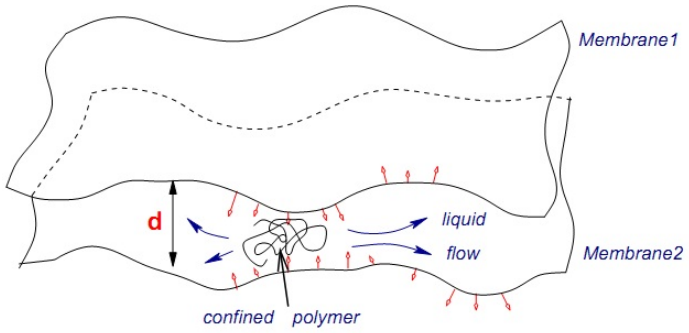

Figure 1.1: **Schematic diagram of a polymer suspended in a fluid confined between two membranes.**

This research work has been motivated by the work done by Raghuveer Parthasarathy and Jay. T. Groves [14] on an experimental system composed of two lipid bilayers with one species of protein sandwiched between them, which gives striking patterns in the protein distribution upon inter-

membrane adhesion. We intend to develop a theoretical understanding of this experiment by looking at a much simpler system which also has relevance to statistical physics of confined polymers. Once this system is thoroughly studied, more complex and biological systems of such kind can be understood. Also the study of such membrane systems could have many industrial applications, such as targeted drug delivery, nanotechnology, and environmental toxicology.

The thesis is organised as following:

In Chapter 2, we give a brief overview of the physics of membranes and polymers and also describe effective models. These models serve as the foundation for the simulations we performed.

In Chapter 3, we describe our simulation models and methods used for the polymer, the membranes and the fluid. We also present results for the three components separately validating our simulation models and thereby, establishing that the models are working accurately.

In Chapter 4, we introduce the coupling thechnique we used to couple the individual components with each other. Then preliminary results obtained from the interacting system are mentioned and discussed. Much of our preliminary results are work in progress.

Finally in Chapter 5, we give future perspectives regarding our study.

Chapter 2

Theoretical models: overview of literature

2.1 Membranes

Cells are the building blocks of all living organisms. They are in turn composed of cell organelles, which have specialised function and structure. However, all cell organelles and the cell itself are enclosed in lipid bilayer membranes. Bilayer membranes separate the exterior environment from the ongoing life processes in the interior. The study of the physics of interfaces and membranes is significant in the context of biological systems. Physicists have tried to characterize the material properties of membranes, e.g. structural parameters like thickness, mechanical constants like bending rigidity and compression modulus.

2.1.1 Membrane composition

Bilayer membranes are formed of a vast variety of components, e.g. phospholipids, cholesterol and proteins etc., in different proportions depending on their function in the cell. Singer and Nicholson proposed in their Fluid Mosaic Model that membranes can be considered as proteins floating in a sea of lipids [15].

Phospholipids: They comprise of a polar head group and two hydrocarbon tails with typical tail length of 14-20 carbons. Membrane thickness and stability of the membrane are regulated by phospholipids.

Cholesterol: It has a small polar head with four planar rings and a relatively short hydrocarbon tail. It has a large influence on the membrane

stiffness with respect to bending and stretching.

Proteins: 20-80% of the membrane mass is made up of proteins and they are attached to the bilayer in various ways. Transmembrane proteins cover both the leaflets of bilayer; glycosyl-phosphatidylinositol (GPI) proteins are bound to one leaflet.

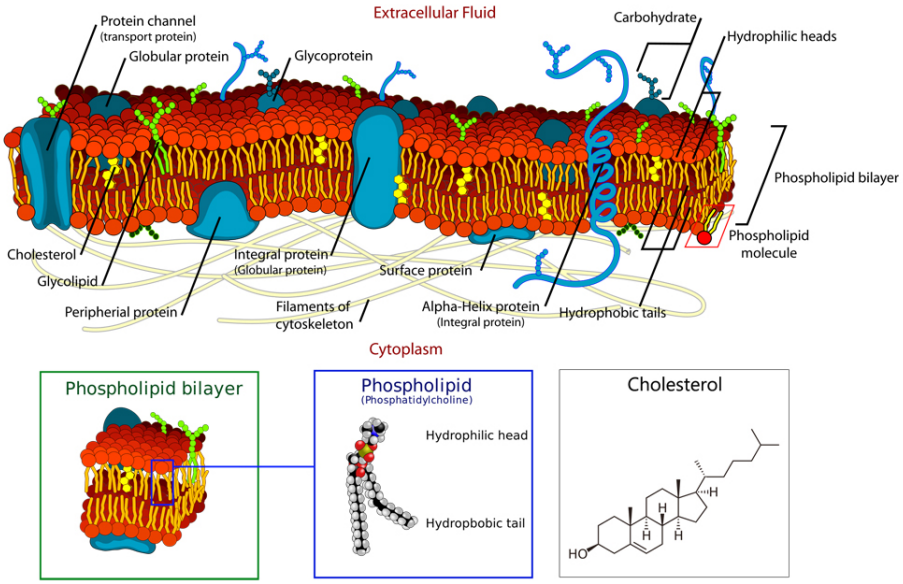

Figure 2.1: **Cell membrane and its components. Images adapted from (http://en.wikipedia.org).**

2.1.2 Properties of membranes

(i) Amphiphilic behaviour of constituents: A lipid molecule consists of two parts, a hydrophilic head and a hydrophobic tail. The hydrophobic part of a lipid molecule do not dissolve in water. That's why lipid molecules form an aggregate to shield its hydrophobic part from the surrounding water by using its hydrophilic head. It is entropically unfavourable to self-assemble, but hydrophobic tails and hydrophilic heads force self assembly of lipid molecules beyond a critical concentration. The hydrophobic interaction which results in repulsion between water and one end of lipid molecule is an effective interaction and its origin can be traced back to decrease in entropy of the water molecule in the presence of hydrophobic molecules.

Lipid molecules can be of different shapes. A single-tailed lipid with comparatively bigger head group is like a cone, while a double-tailed lipid is cylindrical. Cone shaped lipids are more suitable to form spherical aggregates, while cylinders will aggregate mostly into bilayers. The critical shape factors for the formation of aggregates with different shape can be explained through simple geometry [16].

Assume an amphiphilic molecule in an aggregate with head area a, volume v and tail length l. Let the aggregate be spherical with a radius R and made of N amphiphilic molecules. Therefore, we must have $4\pi R^2 = Na$ and $\frac{4}{3}\pi R^3 = Nv$, and from these relations we get $R = \frac{3v}{a}$. Since there is no empty space inside of a micelle, the minimum length of the tail has to be R.

$$l \geq R \tag{2.1}$$

$$P = \frac{v}{la} \leq \frac{1}{3} \tag{2.2}$$

P is referred to as the *packing parameter*. This condition says that spherical aggregate is formed if the packing parameter is smaller than $\frac{1}{3}$. Packing parameter is primarily the aspect ratio of the amphiphile, i.e. a lipid with bigger head and small tail will have a small packing parameter and vice versa.

Similarly aggregation of amphiphile molecules into other geometric shapes yields

$$\frac{1}{3} \leq P \leq \frac{1}{2} \quad \text{(Cylindrical aggregates)} \tag{2.3}$$

$$\frac{1}{2} \leq P \leq 1 \quad \text{(Bilayer aggregates)} \tag{2.4}$$

(ii) Stretching Elasticity: For membrane deformation restricted to the plane, changes to the membrane area is resisted by the stretching modulus. This is due to the hydrophobic cost of exposing the tail groups to the surrounding solvent [17].

Assume a piece of membrane with area A_0 in the state of no external stress. If it is stretched to an area of $A > A_0$ or compressed to an area $A < A_0$, the energy cost for stretching is given by

$$E_{stretch} = \frac{1}{2} K_{stretch} \frac{(A - A_0)^2}{A_0} \tag{2.5}$$

$$\text{Tension,} \quad \Sigma = \frac{\partial E_{stretch}}{\partial A} = K_{stretch} \frac{(A - A_0)}{A_0} \tag{2.6}$$

This is Hook's Law for membrane stretching: stress is proportional to strain. The dimensionless quantity is strain, $u = \frac{A-A_0}{A_0}$ and the proportionality constant $K_{stretch}$ is stretching modulus.

(iii) Bending Elasticity: The bending elasticity resists shape changes due to internal deformations such as chain stretching, distance change of inter head group etc [17]. For a membrane with initial volume V_0, the bending energy can be written as

$$E_{bend} = \frac{1}{2} Y \frac{(V - V_0)^2}{V_0} \tag{2.7}$$

Here, Y is the *Young modulus* for uniaxial extension or compression.

Consider a membrane with dimensions $L_x \times L_y$ and thickness h. The membrane is bent such that it has a radius of curvature $R \gg h$. Consequently, the outer side of the membrane is extended by $(\frac{h}{R})L_x$, the inner side is decreased by same amount and the middle of the membrane remains unperturbed. As we go from $z = \frac{h}{2}$ to $z = -\frac{h}{2}$, the strain varies as $\frac{z}{R}$.

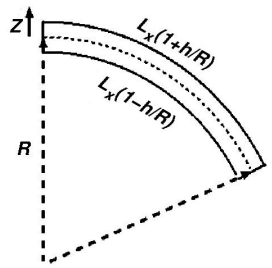

Figure 2.2: **Schematic illustrating membrane bending.**

Therefore, the bending energy per area can be written as

$$\begin{aligned} e_{bend} = \frac{E_{bend}}{L_x L_y} &= \frac{1}{L_x L_y} \int_0^{L_x} \int_0^{L_y} \int_{-\frac{h}{2}}^{\frac{h}{2}} \frac{1}{2} Y \left(\frac{z}{R}\right)^2 dx dy dz \\ &= \frac{1}{2} Y \int_{-\frac{h}{2}}^{\frac{h}{2}} \left(\frac{z}{R}\right)^2 dz \\ &= \frac{1}{24} Y \frac{h^3}{R^2} \end{aligned}$$

This equation can further be written in the form

$$e_{bend} = \frac{1}{2}\kappa\frac{1}{R^2} = \frac{1}{2}\kappa K^2 \tag{2.8}$$

where, K is local curvature and $\kappa = \frac{1}{12}Yh^3$ is bending modulus. κ has the dimensions of energy. The bending energy per area is proportional to curvature (K) so that energy is zero when the membrane is flat ($K = 0$ state) and it does not depend on the sign of the curvature.

2.1.3 Differential geometry of surfaces

A surface is the locus of a point whose coordinates are functions of two independent parameters u,v. Therefore, surfaces in parametric form can be written as

$$x = f(u,v), y = g(u,v), z = h(u,v)$$

By eleminating the parameters u,v the implicit form of surface equation is

$$F(x,y,z) = 0 \tag{2.9}$$

Let $\vec{r}(s)$ be a curve on surface S with curvature κ, unit tanget vector $\hat{t}$ and unit normal $\hat{n}_c$. Then

$$\hat{t} = \frac{d\vec{r}}{ds} \tag{2.10}$$

$$\frac{d\hat{t}}{ds} = \frac{d^2\vec{r}}{ds^2} = \kappa\hat{n}_c \tag{2.11}$$

where, s is the distance in space between two points on the curve.

The *normal curvature*(κ_n) at a point is the curvature of the curve in the direction of the surface normal i.e the projection of curvature on the surface normal.

$$\kappa_n = \kappa\hat{n}_c.\hat{n} = \frac{d^2\vec{r}}{ds^2}.\hat{n} \tag{2.12}$$

where, $\hat{n}$ is the surface normal given by

$$\hat{n} = \frac{\nabla F}{|\nabla F|} \tag{2.13}$$

As one moves a distance $d\vec{r}$ on the surface, the change in surface normal $\hat{n}$ is given by [1]

$$d\hat{n} = Q.d\vec{r} \tag{2.14}$$

In cartesian coordinates,

$$\begin{pmatrix} d\hat{n}_x \\ d\hat{n}_y \\ d\hat{n}_z \end{pmatrix} = \begin{pmatrix} \frac{\partial \hat{n}_x}{\partial x} & \frac{\partial \hat{n}_x}{\partial y} & \frac{\partial \hat{n}_x}{\partial z} \\ \frac{\partial \hat{n}_y}{\partial x} & \frac{\partial \hat{n}_y}{\partial y} & \frac{\partial \hat{n}_y}{\partial z} \\ \frac{\partial \hat{n}_z}{\partial x} & \frac{\partial \hat{n}_z}{\partial y} & \frac{\partial \hat{n}_z}{\partial z} \end{pmatrix} \begin{pmatrix} dx \\ dy \\ dz \end{pmatrix} \tag{2.15}$$

Q is curvature tensor whose elements are given by differentiating Eq. 2.13

$$Q_{ij} = \frac{1}{\Upsilon}\left[F_{ij} - \frac{F_i \Upsilon_j}{\Upsilon}\right] \tag{2.16}$$

where, $\Upsilon = |\nabla F|$, $F_i = \frac{\partial F}{\partial \vec{r}_i}$, $\Upsilon_j = \frac{\partial \Upsilon}{\partial \vec{r}_j}$ and $i, j \in \{x, y, z\}$

Under similarity transformation (eg. rotation) the trace, the sum of principal minors and the determinant of the curvature tensor Q are invariant (appendix A.1). The determinant of Q and one of the eigenvalues are zero. The nonzero eigenvalues are the principal curvatures of the surface. Mean curvature H is the average of the principal curvatures which is twice the value of trace. The product of principal curvatures is called Gaussian curvature K_G, which is the sum of the principal minors of Q. In cartesian coordinates, the curvatures can be expressed as

$$H = \frac{1}{2\Upsilon^3}\left[F_{xx}\left({F^2}_y + {F^2}_z\right) - 2F_x F_y F_{xy} + Perm\right] \tag{2.17}$$

$$K_G = \frac{1}{\Upsilon^4}\left[F_{xx}F_{yy}{F^2}_z - {F^2}_{xy}{F^2}_z + 2F_{xz}F_x\left(F_y F_{yz} - F_z Fyy\right) + Perm\right] \tag{2.18}$$

where, H is the Mean curvature, K_G is the Gaussian curvature, $Perm$ is the other two permutations of (x, y, z).

2.1.4 Helfrich model

In Eq. 2.8, the bending energy of a membrane was written in simple form as a function of the square of local curvature. A more general form of the curvature energy density was proposed by Helfrich [18] in 1973 through symmetry arguments. We have seen in the previous section 2.1.3, the mean curvature and the gaussian curvature are the invariants of surface when it is rotated. So it is appropriate to have them in the energy density expression. The bending energy density proposed by Helfrich has the form

$$\begin{aligned} e_{bend} &= \frac{1}{2}\kappa\left(C_1 + C_2 - C_0\right)^2 + \bar{\kappa}C_1C_2 \\ &= \frac{1}{2}\kappa\left(K - C_0\right)^2 + \bar{\kappa}K_G \end{aligned}$$

where, C_1 and C_2 are the principal curvatures and K is the total curvature.

The *bending modulus* κ measures the energy cost for bending from its equilibrium state and the *saddle-splay modulus* $\bar{\kappa}$ takes care of the saddlelike deformations. Helfrich introduced the term C_0, called as the *spontaneous cuvature*. The bending energy of membrane is minmized for mean curvature value C_0, i.e. membrane is spontaneously curved in its lowest energy state, if $C_0 \neq 0$. It comes into existence when the polar heads of the lipids favour a smaller packing area compared to the hydrocarbon tails and the membrane surface is bent with the heads on the inner side.

2.1.4.1 Gauss-Bonnet theorem

Gauss-Bonnet theorem states that for a boundaryless two-dimensional surface S, the integral of the Gaussian curvature over the entire surface area is 2π times the Euler characteristic of the surface [19].

$$\begin{aligned} \int_S K_G dA &= 2\pi\chi(g) \qquad\qquad [\chi(g) = (2-2g)] \\ &= 4\pi(1-g) \end{aligned}$$

where, g is the total number of handles (e.g. a torus has one handle). It means that even if the surface is distorted and the curvature changes at any location, the total curvature remains invariant. So the Gaussian curvature contribution to the bending energy does not depend on the shape undulation, as long as membrane topology is unchanged.

2.1.4.2 Monge representation

In Monge parametric form [19], $u = x$, $v = y$ and $z = h(u, v) = h(x, y)$ and the surface is represented as $F(x, y, h(x, y)) = z - h(x, y) = 0$, where $h(x, y)$ is the height field above the xy plane. In Monge representation, the mean curvarture and the gaussian curvature can be simplified to

$$H = \frac{(1 + {h^2}_x)\, h_{yy} + (1 + {h^2}_y)\, h_{xx} - 2h_x h_y h_{xy}}{2\left(1 + {h^2}_x + {h^2}_y\right)^{\frac{3}{2}}} \tag{2.19}$$

$$K_G = \frac{h_{xx}h_{yy} - {h^2}_{xy}}{2\left(1 + {h^2}_x + {h^2}_y\right)^2} \tag{2.20}$$

In the small gradient approximation, i.e. for almost flat membrane $h_x \ll 1$, $h_y \ll 1$. In this limit, the mean and gaussian curvature can be written as

$$H \approx \frac{1}{2}\left(h_{xx} + h_{yy}\right) \tag{2.21}$$

$$K_G \approx h_{xx}h_{yy} - {h^2}_{xy} \tag{2.22}$$

Consider a point P on the membrane with coordinates $(x, y, h(x, y))$. Also consider, an parallelogram $\overline{PQRS}$ with Q at a distance dx (in $\vec{x}$ direction) from P and the point S is at a distance dy (in $\vec{y}$ direction). Therefore, Q has coordinates $(x + dx, y, h(x, y) + h_x(x, y)\, dx)$ and S has coordinates $(x, y + dy, h(x, y) + h_y(x, y)\, dy)$. Infinitesimal area element dA of a deformed surface will be given by the area of the parallelogram [1, 16].

$$\begin{aligned} dA &= |\overrightarrow{PQ} \times \overrightarrow{PS}| \qquad \left[\overrightarrow{PQ} = (1, 0, h_x)\, dx, \overrightarrow{PS} = (1, 0, h_y)\, dy\right] \\ &= \sqrt{1 + {h^2}_x + {h^2}_y}\, dxdy \end{aligned}$$

In small gradient approximation, $dA = \left(1 + \frac{1}{2}\left({h^2}_x + {h^2}_y\right)\right) dxdy$.

For a symmetric membrane, there is no spontaneous curvature (C_0) i.e. $C_0 = 0$. Also in section 2.1.4.1 we have seen that Gaussian curvature is not relevant for processes that do not change the topology of the membrane. Therefore, the Helfrich bending energy for a symmetric membrane can be simplified to

$$E_{bend} = \frac{1}{2}\kappa \int_A K^2 dA \tag{2.23}$$

If the membrane has surface tension Σ (takes care of energy cost due to area change when membrane is curved), the energy in small gradient approximation is

$$E_{bend} = \int_A \left[\frac{1}{2}\kappa\left(h_{xx} + h_{yy}\right)^2 + \frac{1}{2}\Sigma\left({h^2}_x + {h^2}_y\right)\right] dxdy \tag{2.24}$$

as the membrane is almost planar, $\int_A \left(h_{xx}h_{yy}\right) dA = 0$

$$E_{bend} = \frac{1}{2}\int_A \left[\kappa\left(h_{xx}^2 + h_{yy}^2\right) + \Sigma\left({h^2}_x + {h^2}_y\right)^2\right] dxdy \tag{2.25}$$

So, we get the most common form of the Helfrich hamiltonian

$$E_{bend} = \frac{1}{2}\int_A \left[\kappa\left(\nabla^2 h\right)^2 + \Sigma\left(\nabla h\right)^2\right] dxdy \tag{2.26}$$

2.1.5 Fluctuation spectrum

Assume a membrane of size $L_x \times L_y$ with periodic boundary conditions and it is described by the height field $h(r)$. The height filed in its fourier series form is

$$h(r) = \sum_q h_q e^{iq.r} \tag{2.27}$$

where, $q = (q_x, q_y) = 2\pi \left(\frac{n_x}{L_x}, \frac{n_y}{L_y}\right)$ with n_x, n_y=0,1,2,....,N (N corresponds to the smallest length scale). Also the Fourier amplitudes obey the symmetry relation $h_{-q} = h^*{}_q$, as the height field $h(r)$ is a real function.

$$\nabla h(r) = \sum_q iq h_q e^{iq.r} \tag{2.28}$$

$$(\nabla h(r))^2 = \sum_{q,q'} (-q.q') h_q h_{q'} e^{i(q+q').r} \tag{2.29}$$

$$\nabla^2 h(r) = \sum_q \left(-q^2\right) h_q e^{iq.r} \tag{2.30}$$

$$(\nabla h(r))^2 = \sum_{q,q'} \left(q^2.q'^2\right) h_q h_{q'} e^{i(q+q').r} \tag{2.31}$$

Using these in the energy expression of Eq. 2.26, we get

$$E_{bend} = \int\limits_{L_x \times L_y} \sum_{q,q'} h_q h_{q'} e^{i(q+q').r} \left[\frac{1}{2}\kappa(q^2 q'^2) + \frac{1}{2}\Sigma(-q.q')\right] d^2r \tag{2.32}$$

using the relation,

$$\int\limits_{L_x \times L_y} e^{-iq.r} d^2r = L_x L_y \delta_{q,0}$$

$$\begin{aligned} E_{bend} &= \sum_{q,q'} h_q h_{q'} L_x L_y \delta_{q+q',0} \left[\frac{1}{2}\kappa(q^2 q'^2) + \frac{1}{2}\Sigma(-q.q')\right] \\ &= L_x L_y \sum_q h_q h_{-q} \left[\frac{1}{2}\kappa q^4 + \frac{1}{2}\Sigma q^2\right] \\ &= L_x L_y \sum_q |h_q|^2 \left[\frac{1}{2}\kappa q^4 + \frac{1}{2}\Sigma q^2\right] \end{aligned}$$

In this energy expression, the contributions from different wave vectors are decoupled, i.e. each value of q corresponds to different degree of freedom. So

using the equipartition theorem, we get

$$L_x L_y \langle |h_q|^2 \rangle \left[\frac{1}{2}\kappa q^4 + \frac{1}{2}\Sigma q^2 \right] = \frac{1}{2} k_B T \tag{2.33}$$

From Eq. 2.33 we obtain the *fluctuation spectrum* of membrane,

$$\langle |h_q|^2 \rangle = \frac{k_b T}{L_x L_y \left[\kappa q^4 + \Sigma q^2 \right]} \tag{2.34}$$

It tells us that fluctuation amplitudes of membrane depend on the temperature T, the bending rigidity κ and the surface tension Σ. It also predicts that for $q > \sqrt{\frac{\Sigma}{\kappa}}$ (small length scale) the fluctuation spectrum is dominated by contribution from bending and for $q < \sqrt{\frac{\Sigma}{\kappa}}$ (larger length scale) tension dominates.

From the fluctuation spectrum, we get the mean square amplitude of membrane fluctuation as [16]

$$\begin{aligned} \left\langle h^2 \right\rangle &= \sum_q \left\langle |h_q|^2 \right\rangle = \sum_q \frac{k_b T}{L_x L_y \left[\kappa q^4 + \Sigma q^2 \right]} \\ &\approx \frac{L_x L_y}{(2\pi)^2} \int_q 2\pi q \frac{k_b T}{L_x L_y \left[\kappa q^4 + \Sigma q^2 \right]} dq \\ &= \frac{k_B T}{4\pi\Sigma} \ln \frac{q_{max}^2 \left(q_{min}^2 \kappa + \Sigma \right)}{q_{min}^2 \left(q_{max}^2 \kappa + \Sigma \right)} \end{aligned}$$

where, we have taken $L_x = L_y = L$ and the integral limits as $q_{min} = \frac{2\pi}{L}$ and $q_{max} = \frac{2\pi}{a}$ (a is the minimum length scale).

For a membrane with negligible tension, we get

$$\begin{aligned} \left\langle h^2 \right\rangle &= \lim_{\Sigma \to 0} \frac{k_B T}{4\pi\Sigma} \frac{q_{max}^2 - q_{min}^2}{\left(q_{max} q_{min} \right)^2} \\ &= \frac{k_B T}{16\pi^3 \kappa} L^2 \end{aligned}$$

So, the standard deviation of fluctuations of a membrane with almost vanishing surface tension is

$$\begin{aligned} \Delta h &= \left[\left\langle h^2 \right\rangle - \left\langle h \right\rangle^2 \right]^{\frac{1}{2}} \\ &= \left[\frac{k_B T}{16\pi^3 \kappa} L^2 \right]^{\frac{1}{2}} \end{aligned}$$

According to the above relation, a membrane with bending rigidity $\kappa = 20k_BT$ will have a standard deviation of 1% of the lateral extension in the limit of no tension.

2.2 Polymer

The word polymer means many parts and refers to polymer molecules consisting of many elementary units, called monomers. Monomers are structural repeating units of polymer connected to each other by covalent bonds. The number of monomers in a polymer is called the degree of polymerization. An important feature of polymers is their architectures, which includes linear chain, branched chain and cross-linked polymer. A branched chain has long and short branches, and a cross-linked polymer is formed of polymer networks. Some polymer molecules are formed of more than one kind of monomers and they are called copolymers.

The statistical physics of polymeric molecules focuses on the universal properties of long chain molecules and is independent of the chemistry of the constituent monomers. We present below some of the simple models used to analyze the static properties and dynamics of polymeric molecules [6, 20, 21, 22].

2.2.1 Ideal polymer chain Model

2.2.1.1 Freely jointed chain

A polymer is rescaled into a freely jointed chain of segment length b such that neighbouring segments are non-correlated. The segment length b is called Kuhn length and there are N such bonds connecting $N + 1$ beads. There is no excluded volume interaction between the monomer beads. The bonds can independently point in any direction and the polymer can cross itself. The end-to-end vector of the polymer is the sum of all N bond vectors in the chain.

$$\vec{R} = \sum_{i=1}^{N} \vec{r}_i \tag{2.35}$$

The average end-to-end vector of an isotropic polymer chain is zero, $\left\langle \vec{R} \right\rangle = 0$. The polymer conformation can be characterized by measuring its mean

square value of $\vec{R}$.

$$\left\langle \vec{R}^2 \right\rangle = \left\langle \left(\sum_{i=1}^{N} \vec{r}_i \right) \left(\sum_{j=1}^{N} \vec{r}_j \right) \right\rangle \tag{2.36}$$

$$= \sum_{i=1}^{N} \sum_{j=1}^{N} \langle \vec{r}_i . \vec{r}_j \rangle = b^2 \sum_{i=1}^{N} \sum_{j=1}^{N} \langle \cos\theta_{ij} \rangle \tag{2.37}$$

The bond directions are not correlated, i.e. the angle between the bonds $\vec{r}_i$ and $\vec{r}_j$ can be of any value from 0 to 2π with equal probability. So, $\langle \cos\theta_{ij} \rangle = 0$ for $i \neq j$ and $\langle \cos\theta_{ij} \rangle = 1$ for $i = j$ and the mean square end-to-end distance becomes

$$\left\langle \vec{R}^2 \right\rangle = Nb^2 \tag{2.38}$$

The above relation holds true for dilute polymer solution at the so called θ temperature when the solvent properties are such that the polymer chain behaves like an ideal chain. Under good solvent conditions where the monomer-solvent affinity is larger than the monomer-monomer affinity $R \sim N^{\nu} b$, where $\nu = 0.6$. This corresponds to the effective description where there are excluded volume interactions between monomers, and chains do not cross each other.

2.2.2 Polymer Dynamics

2.2.2.1 Rouse model

The simplest molecular model of the dynamic behaviour of polymer was developed by P. Rouse in 1953 [23]. Rouse model describes the conformational dynamics of an ideal polymer chain. In this model, the polymer chain is represented as N beads connected by springs with spring constant $k_{sp} = \frac{3k_B T}{b^2}$. The diffusion of the polymer chain is described as Brownian motion of the beads. There is no excluded volume interaction and the beads feel friciton from the background solvent together with thermal noise [20].

The motion of any bead through the solvent induces a velocity field which in turn affects the other beads. This effect is neglected in Rouse model i.e. it does not take care of hydrodynamic interaction. Rouse model works for short chain polymers in melts. In polymer melts the motion of the beads can be thought as oscillation in a local cage, there is no velocity field like in normal solvent meaning that no hydrodynamic interaction.

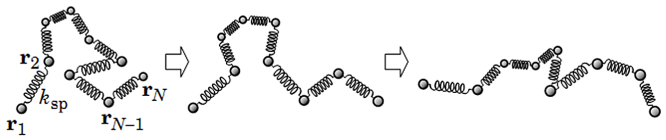

Figure 2.3: **A bead-spring polymer chain changing its conformation with time. Image adapted from Ref. [24].**

Following Langevin dynamics the equation of motion of the nth bead of the polymer chain is written as (appendix B.1)

$$\zeta \frac{\partial}{\partial t}(r_n(t)) = F_n(t) + f_n(t) \tag{2.39}$$

where ζ is the friction coefficient of monomer in the solvent, F_n is the harmonic force acting on monomer n and f_n is random force with $\langle f_n(t) \rangle = 0$, $\langle f_m(t) f_n(t') \rangle = 6\zeta k_B T \delta_{mn} \delta(t - t')$.

The elastic forces on the nth bead are excerted by the two springs connecting the adjacent $(n-1)$th and $(n+1)$th beads, which gives

$$\zeta \frac{\partial}{\partial t}(r_n(t)) = [k_{sp}(r_{n-1}(t) - r_n(t)) + k_{sp}(r_{n+1}(t) - r_n(t))] + f_n(t) \tag{2.40}$$

For a long polymer chain considering the index n as a continuous variable (appendix B.2), Eq. 2.40 takes the form

$$\zeta \frac{\partial}{\partial t}(r_n(t)) = \frac{3k_B T}{b^2} \frac{\partial^2}{\partial n^2}(r_n(t)) + f_n(t) \tag{2.41}$$

For the special case of end monomers we have the following equations of motion

$$\zeta \frac{\partial}{\partial t}(r_1(t)) = \frac{3k_B T}{b^2} (r_2(t) - r_1(t)) + f_1(t) \tag{2.42}$$

$$\zeta \frac{\partial}{\partial t}(r_N(t)) = \frac{3k_B T}{b^2} (r_{N-1}(t) - r_N(t)) + f_N(t) \tag{2.43}$$

with the conditions $r_0 - r_1 \equiv 0, \quad r_{N+1} - r_N \equiv 0$. In the continuous limit, these are equivalent to

$$\left.\frac{\Delta r_n}{\Delta n}\right|_{n=0} = 0, \quad \left.\frac{\Delta r_n}{\Delta n}\right|_{n=N} \tag{2.44}$$

Eq. 2.41 is solved with the boundary conditions using Normal mode analysis. The nth bead position $r_n(t)$ is defined as

$$r_n(t) = x_0(t) + 2\sum_{k=1}^{\infty} x_k(t) \cos\left(\frac{kn\pi}{N}\right) \tag{2.45}$$

Inverting the Eq. 2.45 we get, $x_k(t) = \frac{1}{N}\sum_{n=1}^{N} r_n(t)\cos\left(\frac{kn\pi}{N}\right)$.

We can see that the 0th normal mode describes the center of mass position ($r_G(t)$) of the polymer chain, i.e $x_0(t)$ describes the global motion of the polymer chain, $r_G(t) = x_0(t) = \frac{1}{N}\sum_{n=1}^{N} r_n(t)$. The equations of motion for the normal modes are given by

$$\begin{aligned}\zeta\frac{dx_k}{dt} &= \zeta\frac{1}{N}\sum_{n=1}^{N}\frac{\partial r_n}{\partial t}\cos\frac{in\pi}{N} \\ &= \frac{3k_BT}{Nb^2}\sum_{n=1}^{N}\left[\frac{\partial^2}{\partial n^2}(r_n(t))\right]\cos\frac{kn\pi}{N} \\ &\qquad + \frac{1}{N}\sum_{n=1}^{N} f_n(t)\cos\frac{kn\pi}{N}\end{aligned} \tag{2.46}$$

The first term is

$$\begin{aligned}\sum_{n=1}^{N}\left[\frac{\partial^2}{\partial n^2}(r_n(t))\right]\cos\frac{kn\pi}{N} &\cong \int_0^N\left[\frac{\partial^2}{\partial n^2}(r_n(t))\right]\cos\frac{kn\pi}{N} \\ &= \frac{3\pi^2k_BTk^2}{N^2b^2}\cos\frac{kn\pi}{N}r_n(t)\end{aligned}$$

and Eq. 2.46 is simplified to

$$\zeta\frac{dx_k}{dt} = -\frac{1}{\tau_k}x_k + g_k \tag{2.47}$$

where $\tau_k = \frac{N^2b^2}{3\pi^2k_BTk^2}$ is the mode relaxation time and $g_k = \frac{1}{N}\sum_{n=1}^{N} f_n\cos\frac{kn\pi}{N}$ is the random force of the kth mode with (appendix B.3)

$$\langle g_k(t)\rangle = 0; \quad \langle g_0(t).g_0(t')\rangle = 6\frac{\zeta}{N}k_BT\delta(t-t') \tag{2.48}$$

$$\langle g_k(t).g_l(t')\rangle = 3\frac{\zeta}{N}k_BT\delta_{kl}\delta(t-t') \quad (k\neq 0, l\neq 0) \tag{2.49}$$

Eq. 2.47 for normal modes can be solved as

$$x_k(t) = \frac{1}{\zeta}\int_{-\infty}^{t} g_k(t')\exp\left\{-\frac{t-t'}{\tau_k}\right\}dt' \tag{2.50}$$

The lower limit is taken ∞ considering that polymer chain under Brownian motion loses memory of infintely old past and any assumption can be made

about the initial conditions. The center of mass displacement of the polymer chain at time t is

$$r_G(t) - r_G(0) = x_0(t) - x_0(0) = \frac{1}{\zeta}\int_0^t g_0(t')dt' \tag{2.51}$$

The mean square displacement can be written as

$$\begin{aligned}\left\langle (r_G(t) - r_G(0))^2 \right\rangle &= \frac{1}{\zeta^2}\int_0^t dt_1 \int_0^t dt_2 \left\langle g_0(t_1).g_0(t_2)\right\rangle \\ &= \frac{1}{\zeta^2}\int_0^t dt_1 \int_0^t dt_2 6\frac{\zeta}{N}k_BT\delta(t_1 - t_2) \\ &= \frac{6k_BT}{N\zeta}\int_0^t dt_1 = 6\frac{k_BT}{N\zeta}t\end{aligned} \tag{2.52}$$

From the above Eq. 2.52 we can see that the center of mass of the polymer chain diffuses with diffusion constant $D_G = \frac{k_BT}{N\zeta}$.

The expression for the mean square displacement of each monomer using Eq. 2.45 is given by

$$\left\langle (r_n(t) - r_n(0))^2 \right\rangle = \left\langle (x_0(t) - x_0(0))^2 \right\rangle \tag{2.53}$$

$$+ 4\sum_{k=1}^{N} \left\langle (x_k(t) - x_k(0))^2 \right\rangle \cos^2\left(\frac{kn\pi}{N}\right) \tag{2.54}$$

Using Eqs. 2.52, 2.50 we get

$$\begin{aligned}\left\langle (r_n(t) - r_n(0))^2 \right\rangle &= 6D_Gt \\ &+ \frac{4b^2}{\pi^2}N\sum_{k=1}^{N}\frac{1}{k^2}\left(1 - e^{-tk^2/\tau_1}\right)\cos^2\left(\frac{kn\pi}{N}\right)\end{aligned} \tag{2.55}$$

In the regime $t \gg \tau_1$, i.e. for very large t, the first term will dominate, $\langle (r_n(t) - r_n(0))^2 \rangle = 6D_Gt$. This describes the diffusion of the polymer as a whole with diffusion constant D_G.

Now for $t \ll \tau_1$, replacing the sum over k by integral and $\cos^2\left(\frac{kn\pi}{N}\right)$ by its mean value $\frac{1}{2}$ we get

$$\left\langle (r_n(t) - r_n(0))^2 \right\rangle \cong \frac{2b^2}{\pi^2}N\int_0^\infty dk\frac{1}{k^2}\left(1 - e^{-tk^2/\tau_1}\right) \tag{2.56}$$

with the final result $\langle (r_n(t) - r_n(0))^2 \rangle = \left(\frac{12 k_B T b^2}{\pi \zeta} \right)^{\frac{1}{2}} t^{\frac{1}{2}}$. This tells us that at short time scales the mean square displacement of a typical monomer goes as square root of time t.

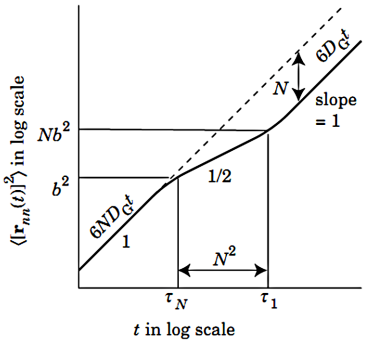

Figure 2.4: **Mean square displacement of the monomer beads on Rouse chain as a function of time t. Image adapted from Ref. [24].**

2.2.2.2 Zimm model

The Rouse model described in the previous section does not incorporate hydrodynamic interactions between different part of a polymer chain and is valid to describe dynamics of unentangled polymer melts. In dilute solutions, hydrodynamic interaction between the monomers and the solvent particles comes into effect. When a monomer bead moves through the solvent, due to viscous resistance solvent particles sorrounding the monomer is also dragged with it, i.e. the velocity field of the solvent becomes perturbed. This induced velocity field affects the frictional force experienced by the other monomers. The polymer dynamics in dilute solutions is described by Zimm model [25], which takes into account the hydrodynamic interactions.

The Langevin equation for the monomers in Zimm model is written as [20]

$$\frac{\partial}{\partial t}(r_n(t)) = \sum_m \overleftrightarrow{\mu}_{nm} . F_m + \rho_n \tag{2.57}$$

where, $\overleftrightarrow{\mu}_{nm}$ is the mobility tensor given by

$$\overleftrightarrow{\mu}_{nn} = \frac{\overleftrightarrow{1}}{\zeta} \quad (n = m); \quad \overleftrightarrow{\mu}_{nm} = \overleftrightarrow{T}(r_n - r_m) \quad (n \neq m) \tag{2.58}$$

$$\overleftrightarrow{T}(r) = \frac{1}{8\pi\eta r} \left(\overleftrightarrow{1} + \hat{r} \otimes \hat{r} \right) \text{ is the Oseen tensor} \tag{2.59}$$

The random stochastic displacements ρ_n have a non-trivial correlation contrary to Rouse model and they satisfy

$$\langle \rho_n(t) \otimes \rho_m(t) \rangle = 2k_B T \overleftrightarrow{\mu}_{nm} \delta(t - t') \tag{2.60}$$

The center of mass diffusion constant of a polymer chain in Zimm model for short-time limit is given by

$$D = \frac{D_0}{N} + \frac{k_B T}{6\pi\eta} \left\langle \frac{1}{R} \right\rangle \tag{2.61}$$

and in the longer time scales this differs slightly. For a long polymer chain, the second term in Eq. 2.61 dominates and we have, $D \propto \frac{1}{R}$. For a polymer chain with $R \sim bN^{\nu}$, this relation yields $D \sim N^{-\nu}$ in accordance with experiments.

The longest relaxation time $\tau_Z \approx \frac{R^2}{D} \approx \tau_0 N^{3\nu}$ implies that the dynamics is faster than Rouse dynamics.

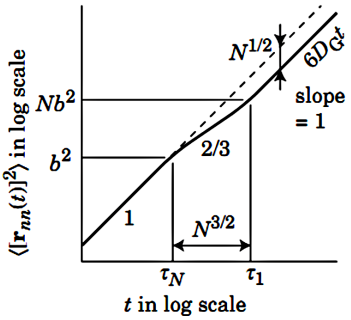

Figure 2.5: **Mean square displacement of monomer beads on polymer chain as a function of time t, for Zimm model. Image adapted from Ref. [24].**

2.3 Conclusion

We have given a very quick overview of physics of polymers and membranes; and we shall use the results from these models to validate systems with interacting polymers and membranes. The physics describing the interaction between membranes/ fluctuating surfaces and polymers while incorporating hydrodynamic interactions becomes more involved and one needs to develop multi-scale simulation methods with explicit coarse grained model of the solvent to start investigating the dynamics of polymers confined between fluctuating surfaces.

Chapter 3

Simulation models and validation

In this chapter, we introduce in greater detail the simulation models and methods we implemented for our three component system. We modeled the membrane as a triangulated mesh surface, the polymer as beads connected by springs and used a particle based coarse grained model for the fluid which captures the combined effect of hydrodynamic and Brownian forces on suspended macromolecules. The phase-space dynamics of the membrane and the polymer is updated using Molecular Dynamics (MD) and for the solvent Multi-Particle Collision Dynamics (MPCD) simulation scheme is implemented and used. To ensure that all the simulation schemes were working perfectly, several physical properties of the polymer, the fluid and the fluctuating membrane were calculated and validated with known theoretical results.

3.1 Molecular dynamics of the membrane

We are interested to study the dynamics of the membrane at larger length scales ($\sim 1\mu$ or more) and not in the atomistic length scale of the constituent phospholipids. The membrane is described by a coarse grained surface model; we use the triangulated surface model with finite bending energy. This model was proposed by Gompper and Kroll in 1996 [26] and this work was futher extended by Noguchi [27]. The membrane comprises of N_{mb} vertices (with mass m_{mb}) forming a tethered triangulated network. The interaction between adjacent vertices are suitably chosen to correctly describe the shape fluctuations of the undulating membrane.

Initially they were positioned in a perfect symmetric lattice formed of equilateral triangles with two neighbouring vertices distance a apart [Fig.3.1].

Initial momenta of the vertices were generated from a uniform random number generator and care was taken such that total momentum of the system is zero and energy per particle is $\frac{3}{2}k_BT$. Next, the time evolution of the membrane system was computed integrating Newton's equation of motion using a discretized Helfrich potential for interaction between the vertices [27].

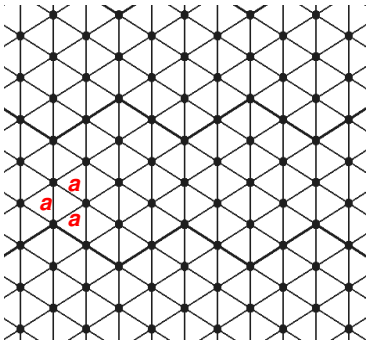

Figure 3.1: **Initial conformation of the triangulated membrane surface formed of equilateral triangles with periodic boundary condition.**

The squared laplacian form of the membrane bending energy as derived in Eq. 2.26 is

$$E_{bend} = \kappa \int dAH^2 = \frac{\kappa}{2} \int dA \left(\nabla^2 h\right)^2 \tag{3.1}$$

The laplacian for a triangulated surface mesh can be discretized [26] and the mean curvature of the surface can be written in the form

$$H_i = \frac{1}{\sigma_i} n_i . \sum_j \sigma_{ij} \frac{\mathbf{r}_{ij}}{r_{ij}} \tag{3.2}$$

where n_i is the surface normal at vertex i and j denotes all the neighbours of vertex i.

From Eq. 3.2 and Eq. 3.1, we get the discetized curvature potential (U^{cv}) used in our simulation

$$U^{cv} = \frac{\kappa}{2} \sum_i \sigma_i (\nabla^2 h)^2{}_i = \frac{\kappa}{2} \sum_i \frac{1}{\sigma_i} \left[\sum_j \sigma_{ij} \frac{\mathbf{r}_{ij}}{r_{ij}} \right]^2 \tag{3.3}$$

where the distance between vertices i and j is r_{ij} and $r_{ij} = |\mathbf{r}_{ij}|$. σ_i is the area of the virtual dual cell of vertex i, given by

$$\sigma_i = \frac{1}{4} \sum_j \sigma_{ij} r_{ij} \tag{3.4}$$

The length σ_{ij} is given by

$$\sigma_{ij} = \frac{r_{ij}}{2} \left[\cot(\theta_1) + \cot(\theta_2)\right] \tag{3.5}$$

where θ_1 and θ_2 are the oppostie angles of the two triangles sharing bond ij (Fig. 3.2).

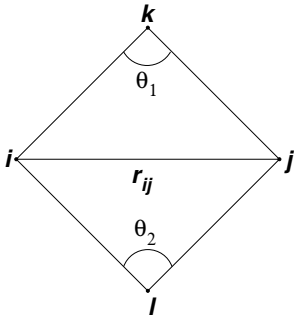

Figure 3.2: **Schematic illustrating the angles θ_1 and θ_2 opposite to the bond r_{ij}.**

In addition to U^{cv} for bending, the bonded and excluded volume interaction between the neighbouring vetices were incorporated with Stillinger Weber potential U^{bond} and U^{rep}, respectively [27]. When the vertices connected by a tether move apart more than cutoff length l_{c0} they attract each other through U^{bond} and at distances less than l_{c1} they repel through U^{rep}. The combination of U^{bond} and U^{rep} keeps the distance of adjacent vertices around a (Fig. 3.3a).

$$U^{bond}(r_{ij}) = \begin{cases} \frac{b \exp\left[a/(l_{c0}-r_{ij})\right]}{l_{max}-r_{ij}} & r_{ij} > l_{c0} \\ 0 & r_{ij} \leq l_{c0} \end{cases} \tag{3.6}$$

$$U^{rep}(r_{ij}) = \begin{cases} \frac{b \exp\left[a/(r_{ij}-l_{c1})\right]}{r_{ij}-l_{min}} & r_{ij} < l_{c1} \\ 0 & r_{ij} \geq l_{c1} \end{cases} \tag{3.7}$$

where $b = 80 k_B T a$, $l_{c0} = 1.15a$, $l_{c1} = 0.85a$. $l_{max} = 1.33a$ and $l_{min} = 0.67a$ are the maximum and minimum bond lengths, respectively.

Integrating the Newtons's equation yields a trajectory that describes the positions, velocities of each particle as they vary with time. We used the Velocity-Verlet algorithm with time step Δt_{MD} to obtain phase-space coordinates [28]. In Velocity-Verlet algorithm the updated position and velocity

are given by

$$\vec{r}(t + \Delta t_{MD}) = \vec{r}(t) + \vec{v}(t)\Delta t_{MD} + \frac{1}{2m_{mb}}\vec{F}(t)\Delta t_{MD}^2 \tag{3.8}$$

$$\vec{v}(t + \Delta t_{MD}) = \vec{v}(t) + \frac{1}{2m_{mb}}\left[\vec{F}(t) + \vec{F}(t + \Delta t_{MD})\right]\Delta t_{MD} \tag{3.9}$$

where force $\vec{F}$ was calculated using Eq. 3.3, Eq. 3.6, Eq. 3.7 as following

$$\vec{F} = \vec{F}^{cv} + \vec{F}^{bond} + \vec{F}^{rep} \tag{3.10}$$

When vertex i moves from position A to position B (Fig. 3.3b), force acts upon it because of the change in its curvature potential U_i^{cv}. The curvature potential for all the six neighbours of i also changes due to the change of the angles contributing to their potentials. Thats why the vertex i feels additional force from its neighbours.

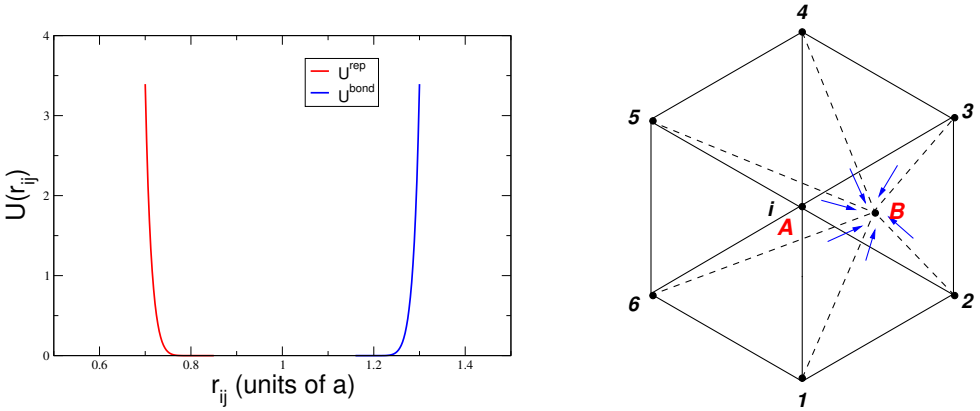

(a) (b)

Figure 3.3: **(a) U^{bond} and U^{rep} which keeps the distance of neighbouring vertices around a. (b) Schematic showing the movement of vertex i from position A to B and the forces acting on it (blue arrows).**

The total force acting on vertex i in $\vec{x}$ direction can be written as

$$F_x^{cv} = -\frac{\partial}{\partial x_i}\left(U_i^{cv} + \sum_k U_k^{cv}\right) \tag{3.11}$$

where, k denotes the neighbours of vertex i, U_i^{cv} is curvature potential of vertex i and U_k^{cv} is curvature potential of k^{th} neighbour.

$$\frac{\partial}{\partial x_i}\left(U_i^{cv}\right) = \frac{\kappa}{2}\left[\frac{1}{\sigma_i}\sum_{l=1,2,3} 2G_l\frac{\partial G_l}{\partial x_i} - \frac{1}{\sigma_i^2}\frac{\partial \sigma_i}{\partial x_i}\sum_{l=1,2,3} G_l^2\right] \tag{3.12}$$

where, j denotes the neighbours of i and $G_l = \sum_j \sigma_{ij} \frac{x_{ij}}{r_{ij}}$ (x_{ij} is distance between i, j in $\vec{x}$ direction).

Similarly as Eq. 3.12 we get $\frac{\partial}{\partial x_i}(U_k^{cv})$ for all the six neighbours of vertex i and using these we find the expression for F_x^{cv}.

$$F_x^{bond} = -\frac{\partial}{\partial x_i}\left(U_i^{bond}\right); \quad F_x^{rep} = -\frac{\partial}{\partial x_i}\left(U_i^{rep}\right) \tag{3.13}$$

Membrane fluidity can be introduced by flipping the bonds between two possible diagonals of two adjacent triangles. Membrane vertices can not easily move away from the cage of its neighbours, if ψ (probability of a particular bond getting flipped) is very less. In our case, we have not incorporated bond flippings, i.e. $\psi = 0$ in our membrane model. Membrane viscosity η_{mb} is high for these type of membrane and they are called solid membrane.

3.1.1 Validation of membrane model

In the MD simulation for membrane, the length and time were scaled according to $\hat{x} = x/a$ and $\hat{t} = t/\tau$, where $\tau = \sqrt{m_{mb}a^2/k_BT}$. All ohter physical quantities of interest were expressed in these units. A membrane of size $64\sqrt{3}a \times 100a$ was taken and we imposed the parameters $k_BT = 1$, $m_{mb} = 1$, $a = 1$, and $\Delta t_{MD} = 0.001\tau$. Periodic boundary condition (PBC) was applied in $\vec{x}$ and $\vec{y}$ direction.

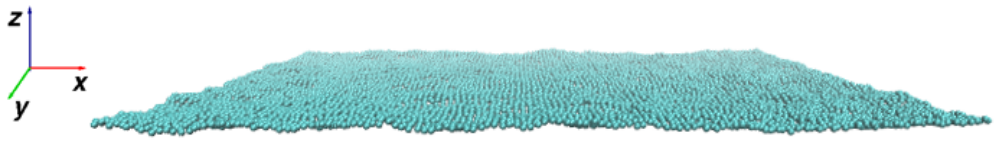

Figure 3.4: **Depiction of the fluctuating membrane with bending rigidity $\kappa = 10k_BT$ from our simulations. PBC has been applied in $\vec{x}$ and $\vec{y}$ direction.**

The membrane system was equilibrated using thermostat at every 50 iterations (Fig. 3.7a). We implemented the Anderson thermostat thechnique which assumes the system to be coupled with a heat bath [28]. The bath acts as a source of thermal energy, supplying or removing heat from the system as needed. In simulations this is done by taking velocity of the system particles from a Maxwell-Boltzmann distribution which represents collision with

an imaginary heat bath. The total energy of the membrane system remains conserved until velocity of the vertices are changed again (Fig. 3.7b).

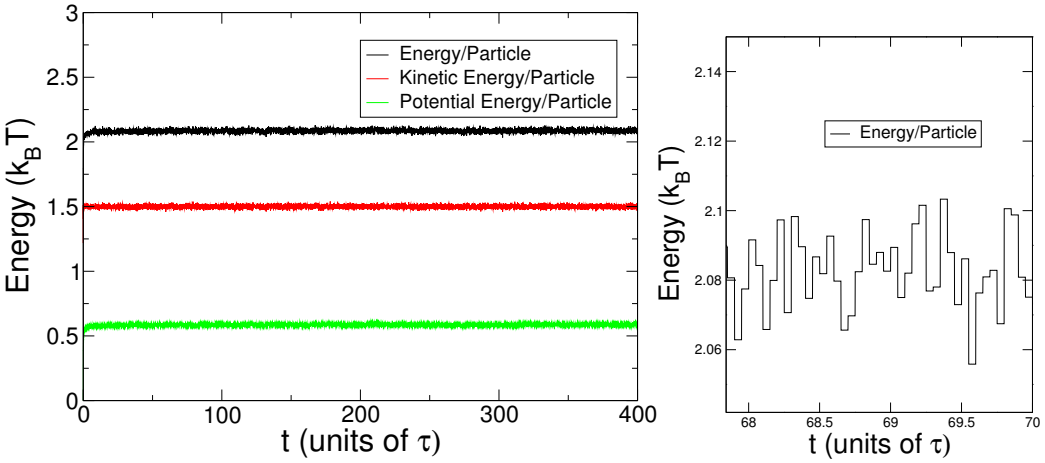

(a) (b)

Figure 3.5: **(a)Plot of the per particle energy, kinetic energy and potential energy of the system after thermostating with temperature $k_BT = 1$, (b)The enegy per particle is zoomed up. It shows that energy is constant in the intermediate 50 iterations.**

The thermal height fluctuations of a membrane is characterized by the fluctuation spectrum. In our MD simulation, fluctuation spectrum $S(q)$ of the triangulated membrane was calculated for membranes with bending rigidity $\kappa = 20k_BT$, $\kappa = 10k_BT$, $\kappa = 5k_BT$ and was averaged over 4 independent runs (Fig. 3.6). Where,

$$S(q) = \left\langle |h_q|^2 \right\rangle \quad \text{with} \quad h_q = \frac{1}{N}\sum_{k=1}^{N} h(r_k)e^{-iq.r_k} \tag{3.14}$$

For a membrane with dimensions $L_x \times L_y$, we considered $q = \sqrt{q_x^2 + q_y^2}$ with $q_x = \frac{2\pi}{L_x}$ to $\frac{2\pi}{a}$ and $q_x = \frac{2\pi}{L_y}$ to $\frac{2\pi}{a}$.

In the small q regime, $S(q)$ increases as q decreases and is well fitted to q^{-4} as predicted by Helfrich theory (Eq. 2.34). It means that long wavelength fluctuations have larger amplitudes, as all fluctuation modes have same energy. After passing through the intermediate regime, there is a peak in the fluctuation spectrum in the large q regime. This maximum is observed at $q = 7.1a^{-1}$ corresponding to wavelength of $0.9a$ which is average distance between two neighbouring vertices. This implies that it is nearest

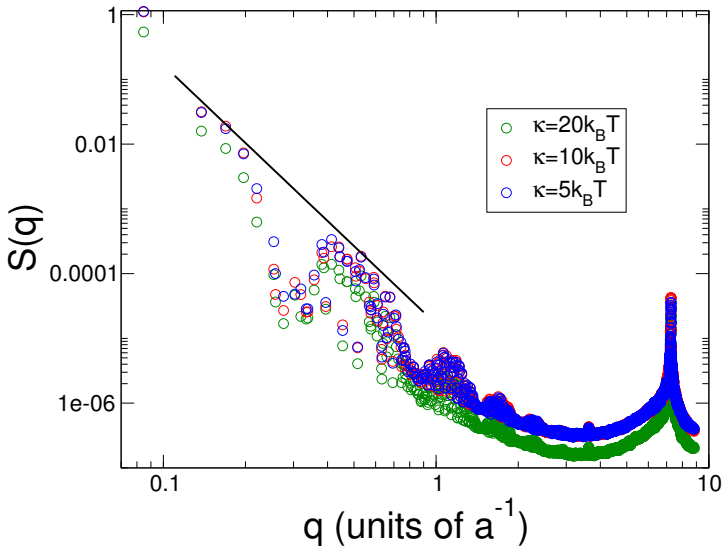

Figure 3.6: **Spectra of undulation modes of membrane with bending rigidity $\kappa = 20k_BT$, $\kappa = 10k_BT$, $\kappa = 5k_BT$. PBC has been applied in $\vec{x}$ and $\vec{y}$ direction. The solid black line represents a slope of q^{-4}.**

neighbour peak of the density structure factor [29, 30, 31, 32]. So, the fluctuation spectrum of membrane undulations can be divided into two parts: pure undulation spectrum in the small q regime and density structure factor contribution dominating in the large q regime.

3.2 Multiparticle collision dynamics of the fluid

We implemented MPCD as a coarse grained model for the fluid dynamics [33]. The fluid is modeled by N_s point particles of mass m_s. Initially, the particles are randomly placed and they are given velocities from a uniform random number generator. Then the MPCD algorithm proceeds in two steps. The *streaming step*, where the particles move ballistically for a time period Δt_{CD} and the position $\vec{r}_i$ of each fluid particle is updated according to

$$\vec{r}_i(t + \Delta t_{CD}) = \vec{r}_i(t) + \vec{v}_i(t)\Delta t_{CD} \tag{3.15}$$

where $\vec{v}_i(t)$ is the velocity of particle i at time t.

Interaction between fluid particles are taken care of in the second part of the algorithm, the *collision step* where clusters of particles undergo collision and their momenta is redistributed. Clusters of particles are identified by sub-dividing the fluid particles into cubic lattice of lattice constant a.

There are total $N_{cell} = \frac{L_x L_y L_z}{a^3}$ ($L_x \times L_y \times L_z$ is the dimension of simulation box) numbers of cubic cells and the average number of particles per cell is $\rho = \langle N_c \rangle = \frac{N_s}{N_{cell}}$ (N_c is the number of particle in cell c). Collision is performed between the particles within a cubic cell and this is done as a stochastic rotation of the velocities of all particles in a cell in its center of mass frame. This step takes care of the momenta exchange among the fluid particles, maintaining energy and momentum conservation. The velocity of particle i after collision is

$$\vec{v}_i^{new}(t + \Delta t_{CD}) = \vec{v}_{cm}(t) + R(\alpha)\left(\vec{v}_i(t) - \vec{v}_{cm}(t)\right) \tag{3.16}$$

where, $\vec{v}_{cm} = \sum_{i=1}^{N_p} \frac{\vec{v}_i}{N_p}$ is the center of mass velocity of the cell particle i is in.

$R(\alpha)$ is the matrix of rotation by an angle α about an axis in the direction of an arbitary unit vector $\hat{u} = (u_x, u_y, u_z)$ and it is given by

$$R(\alpha) = \begin{bmatrix} tu_x^2 + C & tu_x u_y - Su_z & tu_x u_z + Su_y \\ tu_x u_y + Su_z & tu_y^2 + C & tu_y u_z - Su_x \\ tu_x u_z - Su_y & tu_y u_z + Su_x & tu_z^2 + C \end{bmatrix} \tag{3.17}$$

where

$$t = 1 - \cos\alpha; \quad C = \cos\alpha; \quad S = \sin\alpha \tag{3.18}$$

and $\hat{u} = (u_x, u_y, u_z)$ is generated randomly from a uniform distribution for each collision cell.

The thermal velocity of the fluid particles is $v_T = \sqrt{k_B t/m_s}$ and the mean free path is $\lambda = \Delta t_{CD}\sqrt{k_B t/m_s}$. At low temperatures or small time steps, particles diffuses so slowly that they move distance less than a and effectively remain in the same collision cell. Thus, they collide with the same set of particles for many time steps and retain information from previous collisions. Particles become correlated and the molecular chaos assumption is violated.

Galilean inavariance is restored by a random shift of the collision grid before the collision step, as introduced by Ihle and Kroll [34]. This is implemented by shifting all particles in $\vec{x}$, $\vec{y}$ and $\vec{z}$ direction by random vectors with components in the interval $[-\frac{a}{2}, \frac{a}{2}]$. Particles are shifted back to their original positions after the collision is done. This grid shift procedure also accelerates momentum transfer between the collision cells and leads to a collisional contribution to the transport coefficients.

In case of fluid bounded by walls, no-slip boundary condition is ensured by the implementation of bounce-back rule, i.e. the velocities of the fluid particles are reversed when they strikes the wall ($v_i \rightarrow -v_i$) (Fig. 3.7a). Random shift of the collision grid leads to partially filled cells at the walls and the bounce-back rule fails because of that. To restore no-slip boundary condition, ghost particles are added to the cells cut by walls and thus making the total particle number in the cells ρ (Fig. 3.7b) [33]. The velocities of the ghost particles are taken from a Maxwell-Boltzmann distribution with zero mean and variance $N_g m_s k_B T$ (N_g is the number of ghost particles added in the cell).

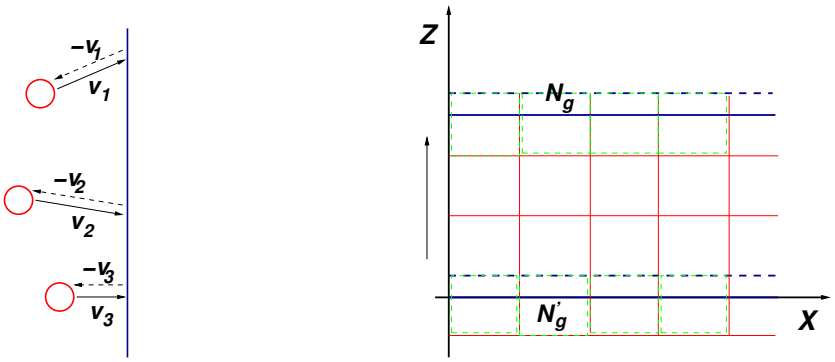

(a) (b)

Figure 3.7: **(a)Depiction of the bounce-back of MPC particles from the wall. The dotted arrows show that the velocity is reversed. (b)Illustration of random shift in Z direction. The dotted blue lines are the boundaries of collision grid after random shifting and green boxes are partially filled cells where ghost particles are added.**

3.2.1 Validation of MPCD scheme

We implemented MPCD simulation scheme for the fluid particles and it was carried out in a $20a \times 20a \times 20a$ simulation box with periodic boundary conditions. The length and time were scaled according to $\hat{x} = x/a$ and $\hat{t} = t/\tau$ with $\tau = \sqrt{m_s a^2/k_B T}$, $k_B T = 1$, $m_s = 1$ and $a = 1$. We also employed the parameters $\alpha = 130°$, $\Delta t_{CD} = 0.1\tau$ and the particle per collision cell $\rho = 10$.

For the establishment that MPCD scheme incorporates proper fluid dynamics following Navier-Stokes equation, we verified few properties of the MPC fluid particles. The speed distribution of the fluid particles was calculated, which was Maxwellian as expected from theory (Fig. 3.8). We of course cross checked local and global energy-momentum conservation of the MPC fluid.

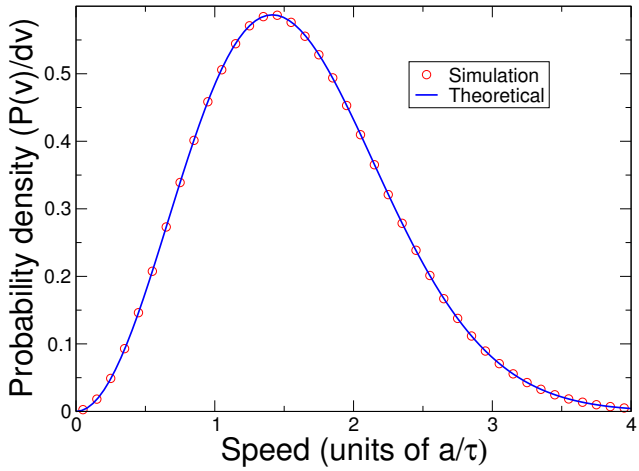

Figure 3.8: **Speed distribution of the fluid particles with the peak at $1.4142a\tau^{-1}$, fitted with the Maxwellian speed distribution curve.**

Analytical expressions for the viscosity η of the MPC fluid has been derived as a sum of the kinetic viscosity η_{kin} and the collisional viscosity η_{coll} [35, 36].

$$\eta = \eta_{kin} + \eta_{coll} \tag{3.19}$$

with

$$\eta_{coll} = \frac{m_s \rho}{18\Delta t_{CD} a}\left(1 - \frac{1}{\rho}\right)(1 - \cos\alpha) \tag{3.20}$$

$$\eta_{kin} = \frac{k_B T \Delta t_{CD} \rho}{a^3}\left(\frac{5\rho}{(4 - 2\cos\alpha - 2\cos 2\alpha)(\rho - 1)} - \frac{1}{2}\right) \tag{3.21}$$

Following Eqs. 3.20, 3.21 the viscosity of our MPCD fluid was calculated to be $\eta = 8.73 k_B T \tau a^{-3}$.

A pressure gradient was applied to the fluid in between two parallel walls to model *Poiseuille flow* and this was done by applying a constant force F in $\vec{x}$ direction on every MPC fluid particle. The position update for $\vec{x}$ direction in the streaming step of MPCD gets modified as

$$r_i^x(t + \Delta t_{CD}) = r_i^x(t) + v_i^x(t)\Delta t_{CD} + \frac{F}{2m_s}\Delta t_{CD}^2 \tag{3.22}$$

To ensure no-slip boundary condition, we also introduced ghost particles in the collision cells near the walls. A parabolic velocity profile was obtained in the Poiseuille flow for suitable forcing (Fig. 3.9). It was ensured that the maximum fluid velocity is well below the speed of sound of the fluid with viscosity $\eta = 8.73 k_B T \tau a^{-3}$, i.e. Mach number, $Ma \ll 1$. Mach number is

the ratio of speed of a particle moving through the fluid and the local speed of sound.

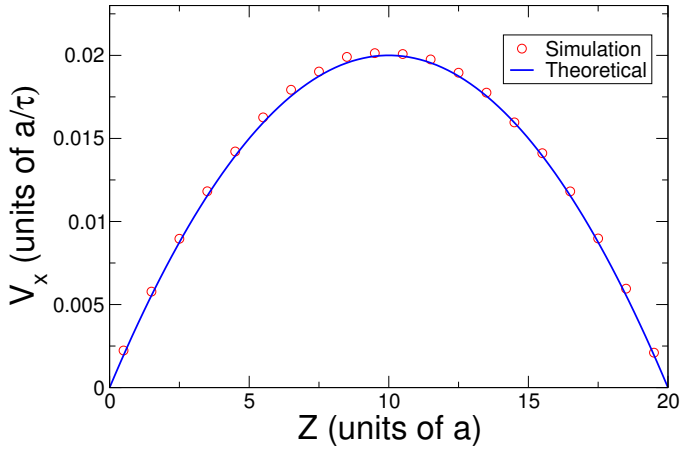

Figure 3.9: **Poiseuille flow velocity profile of the fluid with no-slip boundary condition under pressure gradient $\frac{\partial P}{\partial x} = -0.00348 k_B T a^{-3}$. It is fitted with theoretical curve $v_x = -\frac{\partial P}{\partial x}\frac{1}{2\eta}(L_z z - z^2)$ derived from Navier-Stokes equations. v_{max} for the fluid partcles is $0.02 a\tau^{-1}$, as predicted from theory.**

These results show that MPCD scheme properly models Stokes flow of a fluid.

3.3 Molecular dynamics of polymer

The polymer chain was described as N_p monomer beads of mass m_p each connected through springs [37]. The excluded volume interaction between monomers were modeled using a suitably truncated and shifted Lennard Jones potential which acts when two monomers are within a range of r_c. The range is chosen such that polymer chains can not cross each other.

$$U_{LJ}(r) = \begin{cases} 4\epsilon\left[\left(\frac{\sigma}{r}\right)^{12} - \left(\frac{\sigma}{r}\right)^{6}\right] + f_c r_c - v_c & r < r_c \\ 0 & r > r_c \end{cases} \tag{3.23}$$

where r is the distance between monomers, $f_c = 48\epsilon\left[\left(\frac{\sigma^{12}}{r_c^{13}}\right) - 0.5\left(\frac{\sigma^6}{r_c^7}\right)\right]$ and $v_c = 4\epsilon\left[\left(\frac{\sigma}{r_c}\right)^{12} - \left(\frac{\sigma}{r_c}\right)^{6}\right]$

Consecutive monomers in the polymer chain are connected by a harmonic

spring potential, i.e. the potential models the bonded interaction between the monomers.

$$U_s = k\,(r - r_0)^2 \tag{3.24}$$

where, k is the spring constant, r is the distance between neighbouring monomers and r_0 is the mean bond length.

Using the potentials in Eqs. 3.23 and 3.24, Newton's equations were integrated by the Velocity-Verlet algorithm with time step Δt_p and phase-space dynamics of the polymer was observed.

3.3.1 Validation of polymer model

In the simulations, the length and time were scaled according to $\hat{x} = x/a$ and $\hat{t} = t\sqrt{k_BT/m_pa^2}$ with $k_BT = 1$, $a = 1$. A polymer chain with monomer number $N_p = 40$ was taken and the mass of each monomer was kept $m_p = 1$. We kept $r_0 = a$ and $k = 1000k_BTa^{-2}$ for the harmonic spring potential of the polymer. In the Lennard Jones potential for monomer-monomer interaction $\epsilon = a$, $\sigma = 0.8r_0$, $r_c = 2^{\frac{1}{6}}\sigma$ was employed.

To establish that the MD simulation for the polymer is working properly, we compared the energy plot for two different values of $\Delta t_p = 0.0001\tau$ and $\Delta t_p = 0.0002\tau$ (Fig. 3.10). The fluctuation in energy is 4 times for the later as the energy increase is proportional to Δt_p^2. We also checked energy-momentum conservation as done in the case of membrane.

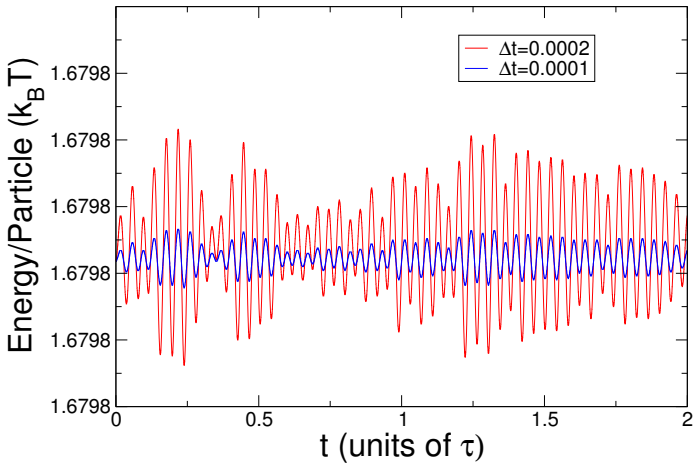

Figure 3.10: **Polymer energy plot for two different values of MD time step Δt_p. For $\Delta t_p = 0.0002\tau$, the fluctuation in energy is 4 times more compraed to $\Delta t_p = 0.0001\tau$.**

We also measured the radius of gyration R_g for polymers of different chain lengths (Fig. 3.11). For a body consisting of N particles R_g is given by $\sum_{i=1}^{N} m_i(r_i - R_{cm})^2 / \sum_{i=1}^{N} m_i$ (m_i is mass of ith constituent particle). As all the monomer beads has identical mass $m_p = 1$, R_g was calculated using

$$\left\langle R_g^2 \right\rangle = \frac{1}{N_p} \sum_{i=1}^{N_p} \left\langle (r_i - R_{cm})^2 \right\rangle \tag{3.25}$$

where, $R_{cm} = \frac{1}{N_p} \sum_{i=1}^{N_p} r_i$ is the center of mass position of the polymer chain.

It was observed that for polymer $R_g \sim N_p^{0.6}$ which is in agree with literature [6].

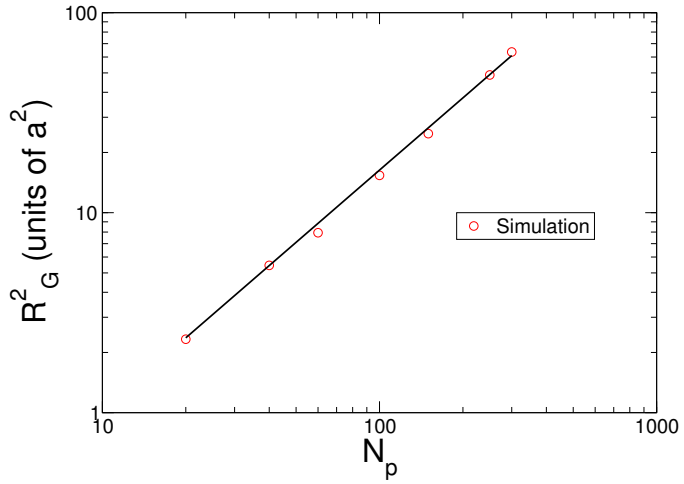

Figure 3.11: **Plot of the radius of gyration square R_g^2 vs monomer number N_p for polymer. The solid black line represents a slope of $N_p^{1.2}$, which implies $R_g \sim N_p^{0.6}$.**

3.4 Conclusion

We discussed the different simulation schemes implemented and showed results validating them in this chapter. We describe the coupling method to combine these simulation schemes in next chapter.

Chapter 4

Multi-scale Simulations: Coupling schemes and Preliminary results

In this chapter, we discuss the coupling scheme we implemented to model the polymer-membrane, membrane-fluid and polymer-fluid interaction and then we present preliminary results obtained from the coupled system. Thermal fluctuations of the membrane are consistently accounted for the coupling scheme. Moreover, the confined MPC fluid imparts Brownian random forces on the membrane as well as the suspended polymer maintaining local momentum conservation; thereby also incorporating hydrodynamic interaction between polymer beads and membrane vertices. In addition there is of course excluded volume interaction between membrane and polymer.

4.1 Coupling method of membrane, fluid and polymer

Polymer-fluid coupling: The hydrodynamic coupling between the polymer monomers and the solvent was modeled by including the monomers in the MPCD collision step with the fluid particles. This assures that there is momentum exchange between the solvent and the polymer.

Polymer-membrane coupling: To ensure that the monomers of the polymer do not penetrate the membranes we incorporated a excluded volume interaction between the membrane vertices and monomers using a suitably truncated and shifted Lennard Jones potential similar to Eq. 3.23.

Membrane-fluid coupling: We modeled the interaction/ momentum exchange of MPC fluid particles with the membrane by combining two schemes,

but keep the membrane surface impermeable to fluid particles [27]. First, the membrane vertices are included in the MPCD collision step and there is momentum exchange with the fluid particles. Second, the fluid particles are scattered from the membrane surface with bounce-back rule so that we obtain no slip boundary condition. The scattering is achieved through the following steps:

(i) In MPCD streaming step, the fluid particles move ballistically for time step Δt_{CD}. We perform the scattering of the fluid particles from membrane surface at a discrete time step Δt_{SC} ($< \Delta t_{CD}$). This implies that the scattering does not happen exactly on the membrane surface, but the fluid particles can possibly penetrate the membrane.

(ii) We assume that the membrane triangles have a small thickness 2δ. After Δt_{SC} time, some of the internal and external fluid particles move within the thickness of the membrane film (particles represented as dotted circles in Fig. 4.1). We identify such particles by calculating the distance of all particles from the triangulated surface and picking those with distance smaller than δ. Only a subset of them undergo collsion.

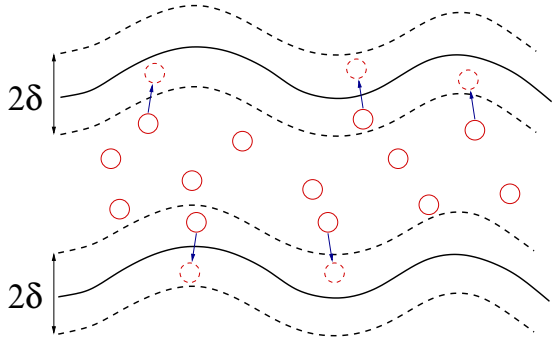

Figure 4.1: **Schematic showing the fluid particles moving within the membrane thickness 2δ at time Δt_{SC}.**

(iii) Next, we distinguish those particles among the above list which have a relative velocity $(\vec{v}_s(t) - \vec{v}_{tri}(t))$ with respect to the membrane triangles such that they move closer to the membrane, where $\vec{v}_s(t)$ and $\vec{v}_{tri}(t)$ are the velocities of the fluid paricle and the center of mass of the membrane triangle, respectively. This is implemented by taking the dot product of $(\vec{v}_s(t) - \vec{v}_{tri}(t))$ and the normal vector $\hat{n}_{tri}$ of the triangle planes around the fluid particles. The fluid particles which will collide with the membrane and those which has already penetrated will have $(\vec{v}_s(t) - \vec{v}_{tri}(t)) . \hat{n}_{tri} < 0$ for some of the

triangles. The normal $\hat{n}_{tri}$ is oriented inward for internal fluid particles and outward for external fluid particles. Only these subset of particles will undergo collision by a scheme which is explained in the next step.

(iv) For each of these particles, we identify the triangle (amongst all those which have $(\vec{v}_s(t) - \vec{v}_{tri}(t)) . \hat{n}_{tri} < 0$) with nearest center of mass from the fluid particle. Then the particle is scattered from the chosen triangle . The scattering was implemented using the bounce-back rule mentioned in Ref. [27] (Fig. 4.2). Momentum and energy of the whole system remains unchanged in this bounce-back process described by Eqs. 4.1, 4.2.

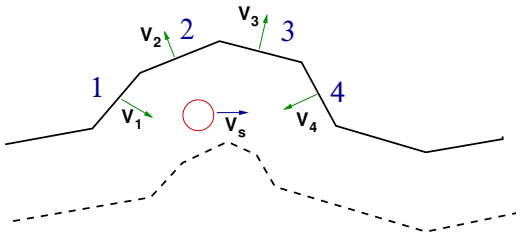

Figure 4.2: **Schematic of the bounce-back of a particle within membrane thickness 2δ. The fluid particle is closer to triangle 1, but it is scattered from the triangle 4 instead of triangle 1 as the relative velocity $(v_4 - v_s)$ is towards the membrane.**

$$\vec{v}_s^{new}(t) = \vec{v}_s(t) - \frac{6m_{mb}}{m_s + 3m_{mb}} (\vec{v}_s(t) - \vec{v}_{tri}(t)) \tag{4.1}$$

$$\vec{v}_{tri}^{new}(t) = \vec{v}_{tri}(t) + \frac{2m_s}{m_s + 3m_{mb}} (\vec{v}_s(t) - \vec{v}_{tri}(t)) \tag{4.2}$$

(v) After this all the fluid particles move ballistically for rest of the streaming step. Also, random shift is not applied in $\vec{z}$ direction for the MPC fluid, as the fluid is bounded by two membranes in that direction.

4.2 Simulation parameters

The length and time were scaled according to $\hat{x} = x/a$ and $\hat{t} = t/\tau$, where $\tau = \sqrt{m_s a^2/k_B T}$. All the other physical quantities of interest were expressed in these units. The two membranes were placed at $L_z^{m1} = \frac{1}{4}L_z$ and $L_z^{m2} = \frac{3}{4}L_z$. The mass of the membrane vertices, polymer monomers were taken to be $m_{mb} = m_p = 10m_s$ with mass of fluid particles $m_s = 1$.

We used the time steps $\Delta t_{CD} = 10\Delta t_{MD}$ and $\Delta t_{SC} = \frac{1}{4}\Delta t_{CD}$ to obtain correct thermal fluctuations. The small membrane thickness used in the interaction between membrane and fluid particle was taken to be $\delta = 0.2a$.

For the Lennard Jones potential of monomer-membrane interaction $\epsilon = 0.2a$, $\sigma = a$ was used.

4.3 Preliminary results

(i) We calculated the fluctuation spectrum $S(q)$ for membranes with fluid confined in between them (Fig. 4.3). It was done for different bending rigidity $\kappa = 20k_BT$, $\kappa = 10k_BT$, $\kappa = 5k_BT$ of the membrane and there was *no polymer* in the fluid. The simulation box had the dimensions $64\sqrt{3}a \times 100a \times 20a$ with the membranes at $5a$ and $15a$. There were total 2.22×10^6 MPC fluid particles with $\rho \sim 10$ particles per collision cell. There is no significant difference with the fluctutation spectra without fluid (Fig. 3.6). The q^{-4} dependence is still observed at small q regime.

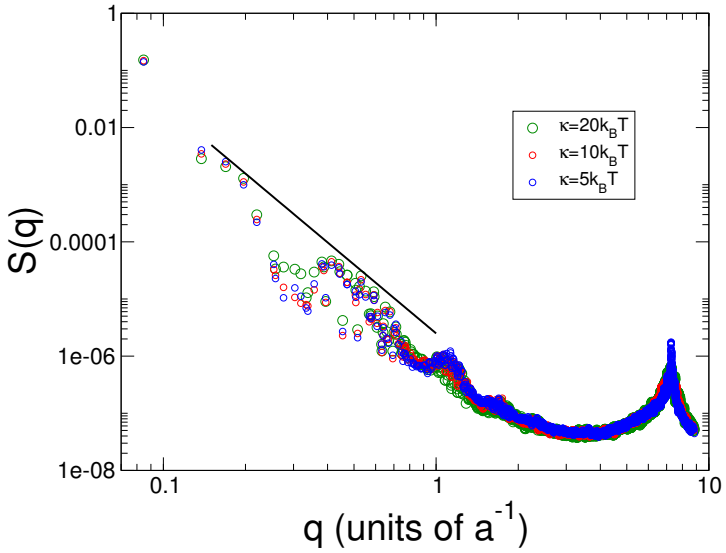

Figure 4.3: **Spectra of undulation modes of membrane with bending rigidity $\kappa = 20k_BT$, $\kappa = 10k_BT$, $\kappa = 5k_BT$ in presence of fluid. PBC has been applied in $\vec{x}$ and $\vec{y}$ direction. The solid black line represents a slope of q^{-4}.**

(ii) We characterized the polymer dynamics when it is suspended in fluid with no bounding surfaces. Mean square displacement (MSD) of the center

of mass and end-to-end vector correlation of the polymer were calculated to compare the results with a polymer confined by membranes. We used a simulation box of dimensions $25a \times 25a \times 25a$ with polymer chain of 50 monomers. There were 1.5625×10^5 number of MPC fluid particles in the box. We allowed 2×10^5 iterations for the system to reach steady state. Data were collected after that for 10^7 iterations, and the MSD and end-to-end vector correlation were averaged over 9 independent runs.

For a polymer chain with excluded-volume interaction, Zimm model predicts the relaxation time in a good solvent as $\tau_{EV}^{Z} \sim N_p^{3\nu} \sim N_p^{1.8}$ for $\nu = 0.6$. We calculated the relaxation time τ_p of the polymer chain using $\tau_p = \eta r_0^2 N_p^{1.8}/k_B T$, where η is the solvent viscosity and r_0 is the mean bond length [38]. We also used $R_g = \frac{r_0}{\sqrt{6}} N_p^{0.6}$ to calculate the radius of gyration R_g of the polymer.

The center of mass mean square displacement (MSD) of a polymer $\langle (\Delta R_{cm})^2 \rangle = \langle (R_{cm}(t) - R_{cm}(0))^2 \rangle \to 6Dt$ as $t \to \infty$, i.e. the polymer diffuses with diffusion constant D at a larger time scale. In our simulations, the linear behaviour of MSD is observed for the polymer at higher t (Fig. 4.4). We also observed the exponential decay of the end-to-end vector correlation function (Fig. 4.5).

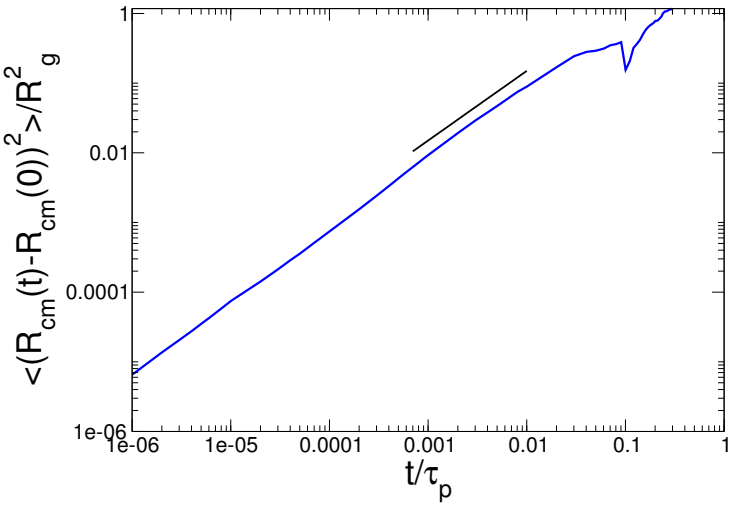

Figure 4.4: **Mean square displacement of the center of mass of a polymer with 50 monomers is plotted as a function of time. The black solid line indicates a slope of** 1**.**

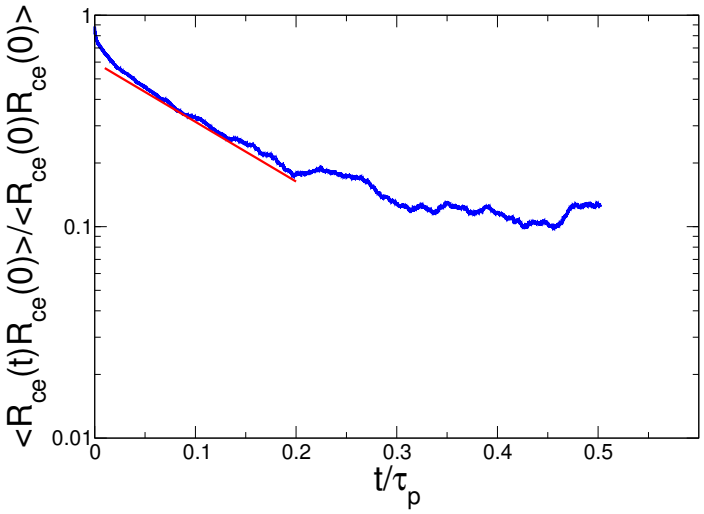

Figure 4.5: **End-to-end vector correlation function of a polymer with 50 monomers vs. time is shown in semi-log plot. The red solid line with slope** -6.5 **is fitted with the curve.**

(iii) Finally, we introduced a polymer of 50 monomers in the MPC fluid confined by two $16\sqrt{3}a \times 30a$ dimensional parallel membranes at a distance $10a$ to observe its dynamics(Fig. 4.6). The time step for MD of membrane and polymer was $\Delta t_{MD} = 0.00125\tau$ with $\Delta t_{CD} = 0.0125\tau$, $\Delta t_{SC} = 0.003\tau$ and the MPC collision was carried out at every 80 MD steps. We observed the total energy of the system which was conserved upto the order of 10^{-3} (Fig. 4.7) ensuring that the three component system is working properly. MSD of the polymer was also calculated by varying the distance d between two membranes (Fig. 4.8a, 4.8b), but averaging over longer time scales is needed to observe proper physics of the polymer under confinement.

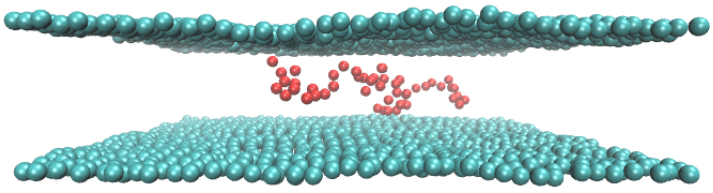

Figure 4.6: **Depiction of the polymer (red coloured) under confinement by fluctuating membranes (cyan coloured) from our simulations. PBC has been applied in** $\vec{x}$ **and** $\vec{y}$ **direction.**

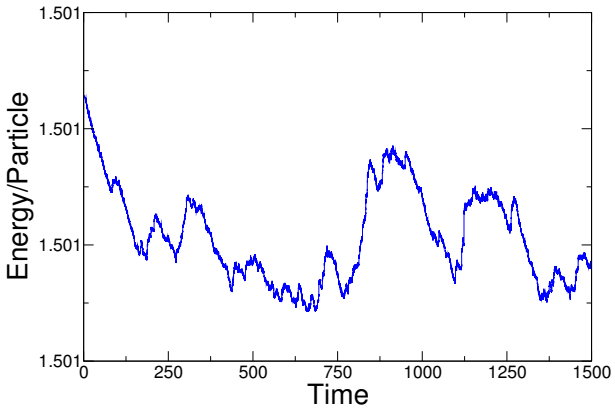

Figure 4.7: **Energy per particle for the three component system. It is constant upto order of 10^{-3}.**

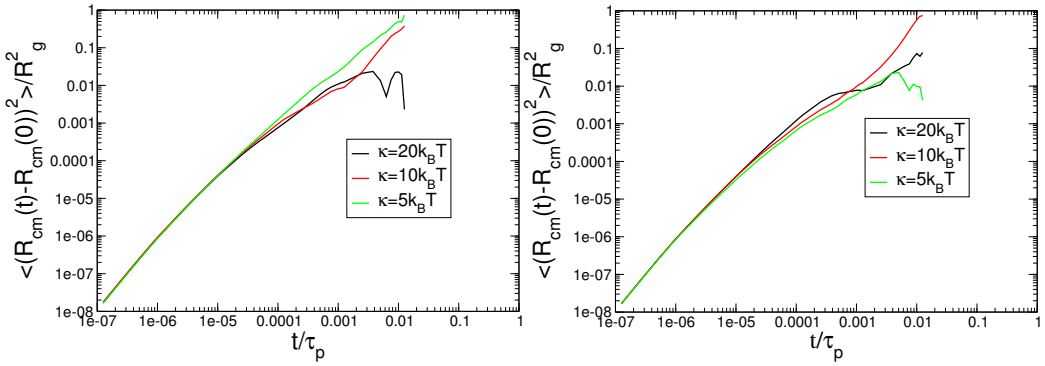

Figure 4.8: **Mean square displacement of the center of mass of a polymer with 50 monomers under confinement by two fluctuating membranes is plotted as a function of time - (a) membrane distance $d = 10a$, (b)membrane distance $d = 6a$. Calculation of MSD over longer time is needed to reach time scales of relevance and interest (work in progress).**

4.4 Conclusion

We have described in detail our implementation of multi-scale simulations combining different schemes which describe the physics of different components each with its own characteristic relaxation time and length scale. Using this scheme, we have started calculating the physical quantities of interest. Runs for much larger iterations and better averaging is needed to reach time scales of relevance and significance.

Chapter 5

Future perspective: Work in progress

We have set up the three component system of two parallel membranes with fluid confined between them and a polymer suspended in the fluid; and some preliminary results have been obtained. Our next goal is to investigate the properties of the coupled system in greater detail to better understand the physics by extending the measurement of already calculated quantities and other properties to time scales and length scales of relevance. Observing the relaxation dynamics will give us insight into the effect of membrane on the polymer behaviour. In particular we want to observe the following:

(i) We intend to study the MSDs of the polymer in lateral x and y directions and compare it with the case of membrane replaced by rigid walls. The difference between MSD in z direction and lateral direction will also be examined.

(ii) We are interested in the change in polymer properties due to the change in membrane bending rigidity κ, i.e. due to the alteration of membrane undulation amplitude.

(iii) We also want to investigate how the confinement affects polymer dynamics, i.e., how the MSD, diffusion constant, other dynamical quantities like dynamic structure factor and certain structural quantities of the polymer varies with the decreasing distance d between the two membranes.

(iv) The effect of polymer dynamics on the membrane dynamics is also a question worth investigating.

References

[1] S. A. Safran, Statistical thermodynamics of surfaces, interfaces, and membranes, Addison-Wesley Reading, MA, 1994.

[2] T. Auth, G. Gompper, Self-avoiding linear and star polymers anchored to membranes, Phys. Rev. E 68 (2003) 051801.

[3] R. Lipowsky, Flexible membranes with anchored polymers, in: Colloids and Surfaces, 1997, pp. 255–264.

[4] T. Auth, G. Gompper, Fluctuation spectrum of membranes with anchored linear and star polymers, Phys. Rev. E 72 (2005) 031904.

[5] W. Sung, S. Lee, The soft-mode instability of a membrane induced by strong polymer adsorption, Europhys. Lett. 68 (2004) 596–602.

[6] P.-G. De Gennes, Scaling concepts in polymer physics, Cornell university press, 1979.

[7] M. Daoud, P. De Gennes, Statistics of macromolecular solutions trapped in small pores, Journal de Physique 38 (1) (1977) 85–93.

[8] K. Kremer, K. Binder, Self-avoiding flexible polymers under spherical confinement, J. Chem. Phys. 81 (1984) 6381.

[9] A. Milchev, W. Paul, K. Binder, Polymer chains confined into tubes with attractive walls: A monte carlo simulation, Macromol. Theory Simul. 3 (1994) 305–323.

[10] A. Milchev, K. Binder, Dynamics of polymer chains confined in slit-like pores, J. Phys. II France 6 (1996) 21–31.

[11] A. Cacciuto, E. Luijten, Self-avoiding flexible polymers under spherical confinement, Nano Letters 6 (2006) 901–905.

[12] J. Kalb, B. Chakraborty, Single polymer confinement in a tube: Correlation between structure and dynamics, J. Chem. Phys. 130 (2009) 025103.

[13] A. Milchev, Single-polymer dynamics under constraints: scaling theory and computer experiment, J. Phys.: Condens. Matter 23 (2011) 103101.

[14] R. Parthasarathy, J. Groves, J. Phys. Chem. B 110 (2006) 8513.

[15] Singer, Nicolson, Fluid mosaic model of structure of cell-membranes, Science 175 (1972) 720.

[16] M. Deserno, Fluid lipid membranes a primer (2007).

[17] W. C. Poon, D. Andelman, Soft condensed matter physics in molecular and cell biology, CRC Press, 2010.

[18] W. Helfrich, Elastic properties of lipid bilayers theory and possible experiments, Z. Naturforsch. C 28 (1973) 693.

[19] T. Auth, Statistical mechanics of membranes, in: J. K. G. Dhont, G. Gompper, G. Nagele, D. Richter, R. G. Winkler (Eds.), Soft Matter from Synthetic to Biological Materials, Vol. 1 of Lecture Notes, Key Technologies.

[20] B. Dünweg, Mesoscopic simulations for problems with hydrodynamics, with emphasis on polymer dynamics.

[21] A. Y. Grosberg, A. R. Khokhlov, Y. A. Atanov, Statistical physics of macromolecules.

[22] K. Kremer, Polymer dynamics: Long time simulations and topological constraints, in: Computer Simulations in Condensed Matter Systems: From Materials to Chemical Biology Volume 2, Springer, 2006, pp. 341–378.

[23] P. E. Rouse, A theory of the linear viscoelastic properties of dilute solutions of coiling polymers, J. Chem. Phys. 21 (1953) 1272–1280.

[24] I. Teraoka, Polymer solutions: An introduction to physical properties, 2002.

[25] B. H. Zimm, Dynamics of polymer molecules in dilute solution: Viscoelasticity, flow birefringence and dielectric loss, J. Chem. Phys. 24 (1956) 269–278.

[26] G. Gompper, D. M. Kroll, Random surface discretizations and the renormalization of the bending rigidity, J. Phys. I 6 (1996) 1305.

[27] H. Noguchi, G. Gompper, Dynamics of fluid vesicles in shear flow: Effect of membrane viscosity and thermal fluctuations, Phys. Rev. E 72 (2005) 011901.

[28] D. Frenkel, B. Smit, Understanding molecular simulation: From algorithms to applications. 2002, New York: Academic.

[29] R. Goetz, G. Gompper, R. Lipowsky, Mobility and elasticity of self-assembled membranes, Phys. Rev. Lett. 82 (1999) 221.

[30] E. Brandt, A. Braun, J. Sachs, J. Nagle, O. Edholm, Interpretation of fluctuation spectra in lipid bilayer simulations, Biophys. J 100 (2011) 2104.

[31] J. Stecki, Correlations in simulated model bilayers, J. Chem. Phys. 120 (2004) 3508.

[32] J. Stecki, Note: On the power spectrum of undulations of simulated bilayers, J. Chem. Phys. 137 (2012) 116102.

[33] G. Gompper, T. Ihle, D. Kroll, R. Winkler, Multi-particle collision dynamics: a particle-based mesoscale simulation approach to the hydrodynamics of complex fluids.

[34] T. Ihle, D. Kroll, Stochastic rotation dynamics: A galilean-invariant mesoscopic model for fluid flow, Phys. Rev. E 63 (2001) 020201(R).

[35] E. Tüzel, M. Strauss, T. Ihle, D. Kroll, Transport coefficients for stochastic rotation dynamics in three dimensions, Phys. Rev. E 68 (3) (2003) 036701.

[36] N. Kikuchi, C. Pooley, J. Ryder, J. Yeomans, Transport coefficients of a mesoscopic fluid dynamics model, J. Chem. Phys. 119 (2003) 6388.

[37] M. P. Allen, D. J. Tildesley, Computer simulation of liquids, Oxford university press, 1989.

[38] D. Ghatage, A. Chatterji, Modeling steady-state dynamics of macromolecules in exponential-stretching flow using multiscale molecular-dynamics-multiparticle-collision simulations, Phys. Rev. E 88 (2013) 043303.

Appendix A

A.1 Invariants of 3×3 matrix

Consider a 3×3 matrix A whose characteristic polynomial is given by

$$P(\lambda) = det(A - \lambda I) \tag{A.1}$$

where, I is the unit matrix

Let $P'(\lambda)$ be the characteristic polynomial after the similarity transformation of $A \rightarrow C^{-1}AC$. Therefore,

$$\begin{aligned} P'(\lambda) &= \left|C^{-1}AC - \lambda I\right| && \text{(A.2)} \\ &= \left|C^{-1}AC - \lambda C^{-1}C\right| && \text{(A.3)} \\ &= \left|C^{-1}(A - \lambda I)C\right| && \text{(A.4)} \\ &= \left|C^{-1}\right| |A - \lambda I| \, |C| && \text{(A.5)} \end{aligned}$$

Using $|C^{-1}| = \frac{1}{|C|}$, we get $P'(\lambda) = P(\lambda)$ i.e. the characteristic polynomial is invariant under similarity transformations.

Now, the characteristic polynomial of a 3×3 matrix A with elements A_{ij} is

$$P(\lambda) = |A| - \lambda \sum_{i=1}^{3} M_i + \lambda^2 \sum_{i=1}^{3} A_{ii} - \lambda^3 \tag{A.6}$$

where, M_i is the principal minor of A.

Since λ is arbitary and $P(\lambda)$ is invariant under similarity transformations, each term in Eq. A.6 is seperately invariant. Thus, the determinant, trace and sum of all the principal minors of any 3×3 matrix are invariant under rotations or other similarity transformations.

Appendix B

B.1 Langevin dynamics of polymer chain

Each monomer bead in Rouse model experiences forces from the neighbouring beads (F), frictional force against the solvent (F^{fr}) and random force (f) appearing when the polymer chain collides with solvent particles. Therefore, the equation of motion of the nth bead can be written as

$$m\frac{\partial^2 r_n}{\partial t^2} = F_n + F_n^{fr} + f_n \tag{B.1}$$

where, $\frac{\partial^2 r_n}{\partial t^2}$ is the acceleration of bead n and m is its mass.

The inertial term in Eq.(B.1) is insignificant for the motion of the polymer chain in a dense solvent. So neglecting this term the equation of motion is

$$F_n + F_n^{fr} + f_n = 0 \tag{B.2}$$

Considering the viscous solvent, in which the monomer beads move with thermal velocities, the frictional force F^{fr} is taken to be proportional to the velocity of monomer beads.

$$F_n^{fr} = -\zeta\frac{\partial r_n}{\partial t} \tag{B.3}$$

Putting this we get the Langevin equation for the polymer chain as,

$$\zeta\frac{\partial r_n}{\partial t} = F_n + f_n \tag{B.4}$$

B.2 Continuous limit of n

If we take the index n (denoting bead no.) as a continuous variable, then we have

$$r_{n+1} - r_n = \frac{\Delta r_n}{\Delta n} \to \frac{\partial r_n}{\partial n} \tag{B.5}$$

$$(r_{n+1} - r_n) - (r_n - r_{n-1}) = \left\{ \left.\frac{\Delta r_n}{\Delta n}\right|_{n=n} - \left.\frac{\Delta r_n}{\Delta n}\right|_{n=n-1} \right\} \frac{1}{\Delta n} \tag{B.6}$$

$$\rightarrow \frac{\partial^2 r_n}{\partial n^2} \tag{B.7}$$

B.3 Correlation of random force g_k

Statistical properties of g_k are similar to f_n

$$\langle g_k(t) \rangle = \frac{1}{N} \sum_{n=1}^{N} \cos \frac{kn\pi}{N} \langle f_n(t) \rangle = 0 \tag{B.8}$$

$$\langle g_k(t).g_l(t') \rangle = \frac{1}{N^2} \sum_{m=1}^{N} \cos \frac{km\pi}{N} \sum_{n=1}^{N} \cos \frac{ln\pi}{N} \langle f_m(t).f_n(t') \rangle \tag{B.9}$$

$$= \frac{1}{N^2} \sum_{n=1}^{N} \cos \frac{kn\pi}{N} \cos \frac{ln\pi}{N} 6\zeta k_B T \delta(t - t') \tag{B.10}$$

$$\cong 6\zeta k_B T \delta(t - t') \frac{1}{N^2} \int_0^N \cos \frac{kn\pi}{N} \cos \frac{ln\pi}{N} dn \tag{B.11}$$

Now,

$$\int_0^N \cos \frac{kn\pi}{N} \cos \frac{ln\pi}{N} dn = \begin{cases} N & (k = l = 0) \\ \frac{N}{2} & (k = l \neq 0) \\ 0 & (k \neq l) \end{cases} \tag{B.12}$$

Therefore,

$$\langle g_0(t).g_0(t') \rangle = 6\frac{\zeta}{N} k_B T \delta(t - t') \tag{B.13}$$

$$\langle g_k(t).g_l(t') \rangle = 3\frac{\zeta}{N} k_B T \delta_{kl} \delta(t - t') \quad (k \neq 0, l \neq 0) \tag{B.14}$$